ACS Biomaterials SCIENCE & ENGINEERING

pubs.acs.org/journal/abseba

Article

Activation of Ibuprofen via Ultrasonic Complexation with Silver in N-Doped Oxidized Graphene Nanoparticles for Microwave Chemotherapy of Cervix Tumor Tissues

Aleksey Drinevskyi, Evgenij Zelkovskyi, Viktar Abashkin, Dzmitry Shcharbin, Tamara Rysalskaya, and Darya V. Radziuk*

Cite This: https://doi.org/10.1021/acsbiomaterials.2c01045

Read Online

ACCESS | Metrics & More | Article Recommendations | Supporting Information

ABSTRACT: An ultrasonic method (20 kHz) is introduced to activate pristine ibuprofen organic molecular crystals via complexation with silver in nitrogen-doped oxidized graphene nanoplatforms (~50 nm). Ultrasonic complexation occurs in a single-step procedure through the binding of the carboxylic groups with Ag, H-bond formation, involving noncovalent $\pi_{C=C} \rightarrow \pi_{C=C^*}$ transitions in the altered phenyl ring and $\pi_{PY} \rightarrow \pi_{CO^*}$ in ibuprofen occurring between the phenyl ring and C−O bonds as a result of interaction with hydroxyl radicals. The ibuprofen−silver complex in ≪NrGO≫ exhibits a ~42 times higher acceleration rate than free ibuprofen of the charge transfer between hexacyanoferrate and thiosulfate ions. The increased acceleration rate can be caused by electron injection/ejection at the interface of the ≪Ag-NrGO≫ nanoplatform and formation of intermediate species $(Fe(CN)_5(CNSO_3)^{x-}$ with $x = 4$ or 5 and $AgHS_2O_3)$ at the excess of produced H^+ ions. Important for microwave chemotherapy, ibuprofen−silver complexes in the ≪NrGO≫ nanoplatform can produce H^+ ions at ~12.5 times higher rate at the applied voltage range from 0.53 to 0.60 V. ≪Ibu-Ag-NrGO≫ NPs develop ~10^5 order higher changes of the electric field strength intensity than free ibuprofen in the microwave absorption range of 100−1000 MHz as revealed from the theoretical modeling of a cervix tumor tissue.

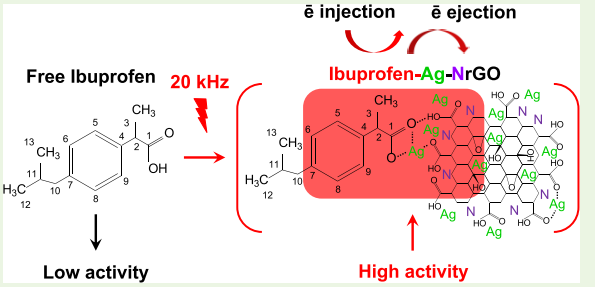

KEYWORDS: *catalysis, NSAID, graphene, microwave chemotherapy, cervix*

1. INTRODUCTION

Ibuprofen (Ibu) is a 2(4-isobutylphenyl)propionic acid from a class of nonsteroidal anti-inflammatory drugs (NSAIDs) with anti-cyclooxygenase properties being used in the treatment of inflammation and associated disorders such as rheumatoid arthritis, osteoarthrosis, ankylosing spondylitis, and degenerative joint disease of the hip. Ibuprofen is associated with significant anti-inflammatory action, effective analgesia, and a comparatively low risk of gastrointestinal tract, renal, hepatic, or infectious side effects in comparison with other NSAIDs. Similar to sulindac and indomethacin, ibuprofen also exhibits antiproliferative effects independent of cyclooxygenase activity,[1] but the mechanisms of these actions remain not fully understood. It is hypothesized that ibuprofen like salicylate and other NSAIDs can alter intracellular processes influenced by Hsc70, which is involved in the processes of cell proliferation, cellular signaling, as well as programmed cell death, indicating another nonoxidative mechanism of its interaction with biomolecules.

Antitumor nanomedicine research has gained much interest because it can provide solutions to better understand the heterogeneity of cancer and produce collective therapeutic effects via different tumor killing pathways.[2] So far, versatile nanoplatforms including different polymeric self-assembled nanocarriers,[3] conjugated polymer-mesoporous nanosilica,[4] and 3D hierarchical nanoflowers[5] have been designed for noninvasive application in external stimuli-triggered multimodal photodynamic therapy by minimizing undesired side effects.[6] As a result, the tumor cell uptake of the therapeutic nanoplatform was improved, the local blood flow was accelerated, oxygenation for relieving tumor hypoxia was raised, and the sensitivity of tumor cells to antitumor drugs was enhanced. However, the uncontrollable premature drug leakage often weakens the therapeutic effects, leading to the increased toxicity. The specific microwave irradiation-induced hyperthermia could modulate the phase transformation of nanoplatform components (CuO, ZrO_2, Au, ZnO, oxidized

Received: September 3, 2022
Accepted: November 15, 2022

graphene, Ag, Ag-rGO, etc.), resulting in a more controlled drug release with a modulated catalytic process of reactive oxygen species (ROS) generation.[7]

Unlike photothermal methods, microwave thermal therapy enables a deeper penetration depth into the tumor tissue and induces high-frequency oscillations ($\sim 1 \times 10^2 - 10^3$ MHz for clinical applications) of intracellular ions and polar molecules.[8,9] However, microwave therapy often leads to the cell necrosis and disintegration of cellular membrane, producing a proinflammatory response caused by the leaked biological components.[10] Over the past few decades, studies have proven the close link between the inflammation and cancer progress, demonstrating a complex interconnected mechanism in which inflammation promotes tumor growth and metastasis.[11] Specifically designed various nanoplatforms based on Ag can provide deeper insights into the local enhancement of microwave sensitization by reduction of inflammation and antimicrobial processes due to the effects of various inorganic and organic components in complexes with drug ligands.[7,12] Microwave conjugation of NSAIDs such as indomethacin, naproxen, and ibuprofen with *N*-benzylamide significantly improves the blood−brain barrier for drug delivery purposes[13] and with acetaminophen and amino acids exhibits more potent anti-inflammatory effects than pristine drugs, but with no visible stomach lesions and no cytotoxicity in animals.[14] NSAIDs exhibit different reduced water solubilities, leading to the rate-limiting dissolution, slow absorption, and poor bioavailability according to the Biopharmaceutics Classification System (BCS).[15] Among NSAIDs, ibuprofen is ascribed to the BCS class II, meaning that its therapeutic efficiency depends on the rate-limiting step of absorption that is the dissolution process. Microwave irradiation of solid dispersions of ibuprofen[16] and also celecoxib,[17] mefenamic, or flufenamic acid[18] causes amorphization of compounds and substantially improves the in vitro dissolution of drug molecules into various polymer-based platforms and in vivo therapeutic efficiency in contrast to untreated NSAIDs.

Distinct from polymers, microwave irradiation is absorbed by carbon atoms with the sp^2-hybridization and induces high dielectric loss in oxidized graphene, resulting in its reduction (rGO) and heating up.[19] Absorbed microwaves in rGO facilitate the formation of various graphene-based nanostructures for applications in nonenzymatic nitrite sensing,[20] long-term antibacterial activity,[21] and improved photocatalysis.[22] Calculated geometry-optimized structures, partial atomic charges, highest occupied molecular orbital (HOMO) and lowest unoccupied molecular orbital (LUMO) energy gaps, work functions, and molecular electrostatic potential data proved that the adsorption process of NSAIDs on rGO is physical in nature (viz., physisorption), primarily as a result of noncovalent $\pi-\pi$ and van der Waals interactions. In this regard, nitrogen-doped rGO−analgesic complexes can exhibit higher adsorption affinities and solvation energies in the gas and aqueous phases.[23] In addition, nitrogen-doped rGO exhibits more enhanced properties and a superior electrocatalytic activity compared to rGO.[24]

Up to now, N-doped rGO was produced by various methods (e.g., N plasma treatment of GO,[25] plasma enhanced chemical vapor deposition PECVD,[26] thermal annealing, pyrolysis, microwave-assisted technique, and different types of hydrothermal methods)[27] and showed enhanced electrocatalytic activity for the reduction of hydrogen peroxide or hydrogen evolution reaction, fast electron transfer kinetics of glucose oxidase, and high sensitivity and selectivity for glucose biosensing. Spin-polarized theoretical studies reveal that the dissociation of O_2 on N-doped rGO is not favorable and the oxygen reduction reaction proceeds with molecular O_2.[28] The oxygen binding and OH bonding energies determine the activity of a surface for oxygen reduction reaction.[29] In this context, Ag exhibits higher activity for oxygen reduction reaction after Pt and Pd and enhanced efficiency for hydrogen peroxide reduction, oxidation, or disproportionation at the contact with N-doped rGO.[30] Therefore, Ag has a potential to be used as a co-catalyst with high-performance metal-free catalysts to improve both the electron conductivity and catalytic efficiency of final nanoplatforms. Among several methods describing the formation of Ag nanostructures on rGO or N-doped rGO surfaces (e.g., femtosecond laser ablation,[31] solvothermal reduction,[32] and sonochemical[33,34] and thermal ultrasound-assisted assembly methods),[35] the ultrasonic technique is more favorable because it provides unique processes of high-energy local gradient enhancement assisted by various mechanical and chemical effects, leading to the formation of highly active final products with finer nanostructure and complex composition at near room conditions.[36] As an advantage shown in our previous studies, ultrasound enables efficient and stable complexation of pristine NSAIDs with metal-based rGO via specific binding and metal−carbon, metal−oxygen, and H-bond formation in a single-step procedure. In another study, it has been shown that ultrasonic irradiation (20 kHz, 40 W/cm^2) can cause fragmentation of organic crystals (45−1000 μm) in the slurry such as pharmaceutically relevant hydrogen-bonding molecules and polycyclic aromatic hydrocarbons via a direct interaction between shockwaves or microjets[37] that is important for the fundamental understanding of sonocrystallization/amorphization in the pharmaceutical science and catalysis. Sonocrystallization has been used to prepare nano- and microcrystals of ibuprofen with improved compressional properties and decreased sticking[38] and other NSAIDs (acetylsalicylic acid[39] and paracetamol[40]).

So far, mainly sonochemical effects of ultrasound have been applied to produce Ag nanowires,[41] Ag/SiO_2 mesoporous nanocomposites,[42] Ag_2S nanospheres,[43] Ag nanoplates,[44] highly fluorescent Ag nanoclusters,[45] Ag-coated papers,[46] Ag/AgCl nanocube plasmonic photocatalysts,[47] and efficient Ag-rGO catalysts.[33] It has been shown that Ag-rGO can be used as an antitumor drug carrier platform of doxorubicin with satisfactory chemo-photo-thermal therapeutic efficacy, tumor targeting property, NIR-controlled drug-releasing function, and X-ray imaging ability;[48] with good antimicrobial activity against the Gram-negative bacteria *Escherichia coli* and *Pseudomonas aeruginosa*;[49] ultrasensitive activity in sensing;[32] enhanced production of thermal energy;[50] and increased electrical conductivity with potential applications in fuel-cell electrodes.[51] In all these studies, the advanced sensing, imaging, and catalytic performance of nanoplatforms arises from the ability of a heterogeneous structure to efficiently transfer electrons to nearby surrounding atoms and molecules, leading to their activation. Therefore, a fundamental understanding of principles of activation of organic molecular crystals in complexes and their relation to charge transfer processes in Ag-based rGO nanoplatforms is important. In this context, the ultrasonic activation of pristine ibuprofen complexed with Ag in N-doped rGO has not been determined yet.

https://doi.org/10.1021/acsbiomaterials.2c01045
ACS Biomater. Sci. Eng. XXXX, XXX, XXX−XXX

2. EXPERIMENTAL SECTION

2.1. Materials and Synthesis. Graphite (dispersity 9.3−47.2 μm, crystallite size 67.7 nm) was purchased from Imerys (France) and has an elemental composition of C = 95.9 ± 10.0 at. %, O = 3.7 ± 0.8 at. %, and Ca = 0.3 ± 0.1 at. %. Silver nitrate ($AgNO_3$, 99.9%), sodium citrate ($Na_3C_6H_5O_7$), H_3PO_4 (85%, higher-grade purity 98%), $KMnO_4$ (higher-grade purity 98%), H_2SO_4 (95%, higher-grade purity 99%), H_2O_2 (60%, higher-grade purity 99%), HCl (35%, higher-grade purity 99%), HNO_3 (40%, higher-grade of purity 99%), ethylene glycol (EG, >98%), polyethylene glycol (PEG, 6000 Da, >98%), NaCl (>98%), salicylic acid (SA, higher-grade purity 99%), ammonium thiocyanate (NH_4SCN, >98%), isopropyl alcohol (C_3H_8O, 99.7%), and ethanol (C_2H_5OH, 96.2%) were obtained from Belreachim JSC (Republic of Belarus). Ascorbic acid (AA, >99%) was obtained from OJSC "EKZON" (Republic of Belarus). Sodium borohydride ($NaBH_4$, >98%) was purchased from Sigma-Aldrich (Germany). Potassium ferricyanide ($K_3Fe(CN)_6$, >99%) and sodium thiosulfate pentahydrate ($Na_2S_2O_3{\cdot}5H_2O$, 99.5%) were purchased from Acros Organics (Belgium). Ibuprofen *per se* (Ibu, 99.5%) was obtained from IOL Chemicals and Pharmaceuticals Ltd. (India). These chemicals were used without any further purification. In all experiments, deionized water (pH 5.5) with a conductivity of less than 5×10^{-6} S·cm^{-1} and a surface tension of 72.2 mN·m^{-1} at 21 °C was used. We synthesized graphene oxide (GO) using the improved Hummers method[52] (more details in the Supporting Information).

2.1.1. Synthesis of N-Doped Oxidized Graphene. The formed GO powder was dispersed at concentrations of 1, 3, 6, 9, and 12 mg/mL in a mixture containing 1 M NH_4SCN and isopropanol by ultrasonic treatment (25 W/cm^2) to obtain a homogeneous colloidal solution. Then, this mixture was separated from the unreacted residual reaction products and washed with deionized water by centrifugation at 4300*g* for 30 min. NH_4SCN (0.01 L, 1 M) was added to the sediment to functionalize GO for 60 min of reaction in a sealed glass flask. Then, this colloidal mixture was thermally treated at T = 87 ± 1 °C for 60 min to form multiple binding sites on the surface of GO. Thermal treatment continued with the temperature increased stepwise to 400 ± 1°C at a rate 5°C/min in the gas atmosphere containing N_2 at 120 cm^3/min and H_2 at 215 cm^3/min for 120 min of reaction during 280 min of annealing. After treatment, the functionalized GO powder turned into a gray-black color and was stored at room temperature. This powder was dispersed in deionized water by ultrasound (7 W/cm^2 for 15 min) and separated from unreacted products by centrifugation at 5100*g* during 15 min. The sediment was diluted by the mixture containing isopropanol and deionized water at a volume ratio of 2:3 and triply washed by centrifugation at 4300*g* during 45 min until pH 5.5 was obtained. The sediment, which is a functionalized oxidized graphene, was dried at 100 °C until a powder with a black color was obtained. The critical concentration of final powder was ∼12 mg/mL, and its aqueous colloidal solution could be stored for at least 6 months.

2.1.2. Complexation of Pristine Ibuprofen with Silver in N-Doped Oxidized Graphene. Ibuprofen *per se* (m = 1.52 g) was dispersed in 0.01 L of ethanol solution (30 wt %) under mechanical stirring in a sealed glass flask for 30 min at room temperature. Then, an aqueous solution of N-doped oxidized graphene (3 mg/mL) and a freshly prepared iced aqueous solution of $NaBH_4$ (0.07 M) were added under continuous mechanical stirring until a homogeneous colloidal suspension was obtained. An aqueous solution of $AgNO_3$ (0.01 M) at a $AgNO_3/NaBH_4$ volume ratio of 1:3 was dropwise added under stirring to this mixture. After complete injection of $AgNO_3$ aqueous solution, the colloidal mixture was ultrasonically treated at 25 W/cm^2 for 20 min in an iced bath. Afterward, this mixture was stored under daylight for 12 h at room temperature. The final products were separated from residual reactants and impurities by centrifugation at 4300*g* for 10 min. The sediment was diluted with deionized water and triply washed by centrifugation until the colloidal solution obtained pH 5.5 and dried to obtain a powder of ≪Ibu-Ag≫ and ≪Ibu-Ag-NrGO≫ nanoparticles.

2.1.3. Formation of Ibuprofen−Silver Complexes in N-Doped Oxidized Graphene with Polyethylene Glycol. PEG-coated nanoparticles of ibuprofen−silver complexes in N-doped oxidized graphene were synthesized according to protocols A and B described below.

2.1.3.1. Protocol A. At first, a seed mixture was prepared. This mixture was composed of 0.02 L of an aqueous solution of N-doped oxidized graphene (2.5 mg/mL) in isopropanol (50 wt %). This colloidal solution was diluted by salicylic acid *per se* (m = 0.05 g) acting as a reductant of nanoparticles in a thermoisolated glass flask during ultrasonic treatment at 25 W/cm^2 for 15 min in an iced bath. The pH of this sonicated mixture was 7.0. The reaction product was separated by centrifugation at 6150*g* for 5 min, and the supernatant was carefully removed. The sediment was dispersed in 0.01 L of isopropanol (50 wt %); dropwise added 0.001 L of $AgNO_3$ (0.01 M), 0.011 L of the mixture composed of polyethylene glycol and dimethylformamide (5 mg/mL), and 0.003 L of iced aqueous solution of $NaBH_4$ (0.07 M); and ultrasonically treated at 20 W/cm^2 for 20 min in an iced bath. In a separate procedure, a reaction mixture was obtained. It was prepared by stirring of a solution composed of 0.005 L of $AgNO_3$ (0.01 M) and 0.013 L of polyethylene glycol in dimethylformamide (5 mg/mL). Then, this solution was diluted by 0.001 L of NH_4SCN (1 M) in isopropanol (50 wt %) and ultrasonically treated for 5 min. Finally, the seed solution was placed in an Erlenmeyer glass flask (0.05 L) and diluted by 0.006 L of isopropanol (50 wt %) under stirring. Then, the reaction solution was added to it, and the obtained mixture was ultrasonically treated (25 W/cm^2) for 20 min. The sonicated mixture was stored at room temperature for 12 h. The product was separated from the unreacted residuals and impurities by centrifugation at 4300*g* for 15 min. The sediment was dispersed in deionized water (pH 5.5) and triply washed by centrifugation at the same conditions until the pH of the colloidal solution was 5.5.

A freshly prepared iced aqueous solution of $NaBH_4$ (0.07 M) and $AgNO_3$ (0.01 M) at a volume ratio of silver cations to borohydride ions of 1:3 was added to a solution of ibuprofen (20 mg/mL) in isopropanol under stirring. This mixture was ultrasonically treated (25 W/cm^2) for 20 min and turned from black to transparent violet-raspberry with a dark sediment at the bottom. The sediment was separated from the mother solution by centrifugation at 4100*g* for 15 min, dispersed in deionized water (pH = 5.5), and doubly washed by centrifugation at the same conditions until the pH of the colloidal solution was 5.5. Control experiments were performed with ibuprofen without silver or N-doped oxidized graphene.

2.1.3.2. Protocol B. At first, the mixture containing three components—ibuprofen *per se* (40 mg/mL), $AgNO_3$ (0.05 M), and N-doped oxidized graphene (1 mg/mL)—was prepared at a volume ratio 1:1:1 under stirring and thermally treated at T = 60 °C for 10 min. Then, 15 mL of this mixture was added to 45 mL of $NaBH_4$ (0.035 M) under stirring, resulting in a color change of the final solution from black-brown to green-brown due to the reduction of silver at the contact with N-doped oxidized graphene. The sediment was separated from the mother solution by centrifugation at 3250*g* for 15 min. The supernatant was carefully removed, and 10 mL of the obtained sediment was diluted by 20 mL of polyethylene glycol stock solution (5 mg/mL in 0.5 M NaCl). The mixture turned first into black tea color and, after thermal treatment at T = 90 °C for 20 min, changed its color into pale yellow. The sediment was removed from the mother solution by centrifugation at 3250*g* for 15 min and resuspended with ethanol solution (30 wt %) at a volume ratio 1:2. Control experiments were performed with ibuprofen *per se* and ibuprofen with adsorbed silver cations without N-doped oxidized graphene. Alternatively, the temperature in the thermal treatment was reduced to 40 °C, and sonication (25 W/cm^2, 10 min) was carried out to enhance the interaction of pristine ibuprofen with silver cations, polyethylene glycol, and N-doped oxidized graphene.

2.1.4. The Catalytic Activity of Nanoparticles. The electron-transfer reaction between 200 μL of 0.01 M $Fe(CN)_6^{3-}$ and 200 μL of 0.1 M $S_2O_3^{2-}$ was chosen to examine the electrokinetic activity of 600 μL of formed ≪Ibu-Ag-NrGO≫ in comparison with ≪Ibu-Ag≫ nanoparticles or pristine ibuprofen (5 mM, 30 wt %). Control experiments were performed with nanoparticles without ibuprofen:

https://doi.org/10.1021/acsbiomaterials.2c01045
ACS Biomater. Sci. Eng. XXXX, XXX, XXX−XXX

≪Ag-PEG≫, ≪Ag-NrGO-PEG≫, ≪Ag-NrGO≫, ≪Ag-rGO≫, and bulk 5 mM $AgNO_3$ aqueous solution. The absorbance spectra of these aqueous colloidal solutions were measured using a Jasco V-630 spectrophotometer with an operating range from 190 to 1100 nm, wavelength setting accuracy of ±0.2 nm, and reproducibility of ±0.1 nm at 25 °C. The decline of the $Fe(CN)_6^{3-}$ peaks with and without NPs as a function of time was monitored by the absorption at ≈420 nm. The kinetics of the electron transfer during this reaction was examined every 5 min of reaction. Always, freshly prepared hexacyanoferrate(III) and thiosulfate aqueous solutions were used in each kinetic run.

2.1.5. Theoretical Modeling of the H^+ Production in NPs. In this model free ibuprofen, ≪Ibu-Ag≫ and ≪Ibu-Ag-NrGO≫ NPs are located in close proximity to the surface of a platinum electrode with an anode radius of 1 mm being inserted into the cervix tumor tissue during the electrolysis. In the electrolysis, the current yield of electrochemical reactions changes at the contact with pristine ibuprofen and NPs and can be modulated by the applied voltage. In the electrolysis, electrochemical reactions lead to the formation of toxic species that can be differently sensed by tumor and healthy tissues. If the anode material contains metal NPs, which can be passivated, i.e., coated with a thin oxide layer, this oxide film acts as a barrier to the anodic metal dissolution reaction. Among the main reactions is the decomposition of water:

$$2H_2O \leftrightarrow O_2 + 4H^+ + 4e^-$$

The following hydrogen evolution reaction was considered in the cathode model:

$$2H_2O + 2e^- \leftrightarrow H_2 + 2OH^-$$

The solution near the electrode is assumed to be saturated with hydrogen. Small hydrogen gas bubbles, with an internal pressure of 1 atm, are assumed to be in equilibrium with the platinum electrode surface.

Because convective transport is obstructed by the dense structure of tissues, species produced at the anode and cathode are mainly transported to the surrounding tissue by diffusion due to concentration gradients and by migration (charged species) due to the potential gradient. The electric field influences the ion exchange across the cell membranes and thereby the conditions for many essential enzyme-regulated reactions. It is suggested that the electrochemical reaction products may also react with organic and inorganic tissue constituents.

The mathematical modeling is based on the fundamental Nernst−Planck equation interface with application to a cervix tissue surrounding a spherical Pt electrode under a continuous direct current. The aim of this model is to calculate the produced amount of H^+ ions by free and complexed ibuprofen compounds in the electrolysis of tumor tissue. The electrolyte domain is bounded by an inner and outer spherical surface. The inner boundary surface represents the spherical electrode with a radius ≈ 1 mm. The outer boundary represents a spherical surface with a radius at a distance large enough from the electrode to ensure constant concentrations. The following domain equations were used:

$$\frac{\partial C_i}{\partial t} = -\Delta \cdot N_i + R_i,$$

where C_i is the concentration, t is the time, N_i is the molar flux, and R_i is the value of prediction species through homogenous chemical reactions. R_i is directly related to the kinetics of the chemical reactions that occur in the electrolyte domain.

The molar flux vector was expressed as

$$N_i = -D_i \Delta C_i - \frac{Z_i}{|Z_i|} u_i C_i \Delta \Phi,$$

where D_i is the diffusion coefficient, Z_i is the number of charges carried by the ion i, u_i is the ionic mobility, and Φ is the potential field in the electrolyte.

The kinetics of the chemical reactions for OH^- production in the anode modeling was considered as

$$R_{OH} = -k_f C_H{}^+ + C_{OH}{}^- + k_b C_{H2O},$$

where k_f and k_b are the forward and backward rate constants of the water pyrolysis reaction and C_H, $C_{OH}{}^-$, and C_{H2O} are the concentration values of H^+ and OH^- ion production and of water molecules.

In the model, the electrode is assumed to be placed at a distance far enough from its opposite to ensure that the anodic and cathodic reaction zones do not interact. When current is applied to tissues, it is mainly transported through the channels of extracellular fluid as confirmed by the electro-osmotic effects, which have been shown to arise during the electrolysis.[53] It is considered that the current is carried by diffusible ions in the extracellular fluid and substantial concentration gradients of these ions arise during electrolysis. Due to the transport of solutes across the cell membranes, changes in extracellular concentrations also affect the composition of electrolytes in the intracellular compartment. However, the nature and time dependence of this interplay during the electrochemical treatment are poorly understood. Transport of current is assumed to occur solely through the extracellular fluid in this work. The tissue is treated as a dilute and homogeneous aqueous solution, so no consideration is taken of the fact that, in real tissues, the cells serve as obstacles for transport of species in the extracellular fluid. Hence, the transport properties of the involved species are approximated to being those found in aqueous solutions. Two transport mechanisms, diffusion and migration, are assumed to contribute to the transport of the solute species in the tissue. The flux of species due to convection is neglected. This assumption is justified as convection is strongly obstructed by the dense structure of tissues. The electro-osmotic and gas bubbles effects in tissues surrounding the electrodes are negligible in the electrolyte and are not considered in the analysis. In reality, the electric field causes a flux of extracellular water from the anode toward the cathode, and consequently, the tissue surrounding the anode dehydrates, whereas edema occurs around the cathode.

The COMSOL Multiphysics software tool was used to compute the concentration of H^+ ions in close proximity of the anode electrode surface with free ibuprofen or produced NPs in the domain at different time steps from 0 to 3600 s. In the computation we used, the potassium chloride model with a diffusion coefficient of K (D_K) = 1.84×10^{-9} m^2/s, diffusion coefficient of H^+ (D_H) = 9.31×10^{-9} m^2/s, mobility of K ≈ 7.43×10^{-13} (S mol)/kg, mobility of H^+ ≈ 3.76×10^{-12} (S mol)/kg, initial concentration of KCl (C_{KCl})= 4.76 mol/L, and initial concentration of H+ (C_H) = 1×10^{-7} mol/L. An initial total current density (j_{tc}) = 100×10^{-9} A/m^2 was applied in the model. The initial anode potential was −0.5 V, the initial equilibrium anodic potential of hydrogen production was 0.53 V, and the equilibrium cathodic potential of oxygen evolution was 1.2 V. The mathematical modeling was performed in the range of applied potential from 0.53 to 0.60 V with a step of 0.01 V. The variables were the exchange current density on the surface of free ibuprofen at the anode (j_a(Ibu) = 78.0×10^{-9} A/m^2) and cathode (j_c(Ibu) = 186.0×10^{-9} A/m^2) and the following NPs with an average diameter of 10 nm: ibuprofen-silver (j_a(Ibu-Ag) = 6.1×10^{-9} A/m^2 and j_c(Ibu-Ag) = 14.6×10^{-9} A/m^2), ibuprofen-AgNrGO (j_a(Ibu-AgNrGO) = 0.1×10^{-9} A/m^2 and j_c(Ibu-AgNrGO) = 0.3×10^{-9} A/m^2), Ag (j_a(Ag) = 1435.0×10^{-9} A/m^2 and j_c(Ag) = 3444.0×10^{-9} A/m^2), and Ag-NrGO (j_a(Ag-NrGO) = 0.8×10^{-9} A/m^2 and j_c(Ag-NrGO) = 1.9×10^{-9} A/m^2).

2.1.6. Theoretical Modeling of the Electric Field Strength Intensity and Power Flow Density Distribution of Nanoparticles in Cervix Tissues under Microwave Irradiation. The mathematical modeling was performed using the COMSOL Multiphysics 4.3 software program. This model computed the electromagnetic radiation field distribution in relation to the electrical conductivity of ultrasonically formed ≪Ibu-Ag≫ ≪Ibu-Ag-NrGO≫ NPs in comparison with free ibuprofen under microwave irradiation in the frequency range from 100 MHz to 1 GHz. This model is related to the area of microwave chemotherapy of oncological disorders, and it

https://doi.org/10.1021/acsbiomaterials.2c01045
ACS Biomater. Sci. Eng. XXXX, XXX, XXX−XXX

computes the electromagnetic field developed by NPs coupled to the bioheat equation of a cervix tissue. It is supposed to selectively irradiate a deep-seated cervix under conditions of reduced damage to the surrounding healthy tissues via insertion of a thin microwave coaxial slot antenna into the tumor.[54] The penetrated microwaves heat up the tumor inside out, producing a coagulated region where the cancer cells can be killed.

In this model, the frequency-domain problem was formulated assuming the unknown complex-valued azimuthal component of the electromagnetic field. The interior of the metallic components of NPs was not modeled. Instead, the mathematical modeling computed the boundary conditions, setting the tangential component of the electric field to zero. It was assumed that time-harmonic electromagnetic fields have complex amplitudes as described by the following equations:

$$E = e_r \frac{C}{r} e^{j(\mathrm{wt}-\mathrm{kz})}, \quad (1)$$

$$H = e_\phi \frac{C}{rZ} e^{j(\mathrm{wt}-\mathrm{kz})}, \quad (2)$$

where E and H are the electric ($\mathrm{kg{\cdot}m{\cdot}(s^3{\cdot}A)^{-1}}$) and magnetic ($\mathrm{N{\cdot}s{\cdot}(C{\cdot}m)^{-1}}$) field components; C is the specific heat capacity ($\mathrm{J{\cdot}(kg{\cdot}K)^{-1}}$); r, φ, and z are the cylindrical coordinates centered along the coaxial axis; Z is the wave impedance in the dielectric part of NPs; r is the radius of NPs; ω is the angular frequency; and κ is the propagation constant ($2\pi/\lambda$, λ is the wavelength in nm).

The following wave equation was applied:

$$\nabla\left(\left(\varepsilon_r - \frac{j\sigma}{\omega\varepsilon_0}\right)^{-1} \nabla \mathrm{x} H_\phi\right) - \mu_r {\kappa_0}^2 H_\phi = 0, \quad (3)$$

where ε_r is the relative permittivity (complex dielectric constant), ε_0 is the absolute dielectric permittivity ($\mathrm{s^4{\cdot}A^2{\cdot}\ kg^{-1}{\cdot}m^{-3}}$), σ is the electric conductivity ($\mathrm{S{\cdot}m^{-1}}$), μ_r is the relative magnetic permeability, and κ_0 is the thermal conductivity at one bar 10^5 $\mathrm{N{\cdot}m^{-2}}$ ($\mathrm{W{\cdot}(m{\cdot}K)^{-1}}$) of NPs and cervix tissues.

The boundary conditions for the metallic surfaces in the antenna were the following:

$$n \times E = 0, \quad (4)$$

and the feed point was modeled using a port boundary condition with the power level set to 10 W. In the model, the stationary heat transfer problem was computed as

$$\nabla(-\kappa \nabla T) = \rho_{\mathrm{blood}} C_{\mathrm{blood}} \omega_{\mathrm{blood}} (T_{\mathrm{blood}} - T) + Q_{\mathrm{cervix}}, \quad (5)$$

where κ is the cervix's thermal conductivity ($\mathrm{0.53\ W{\cdot}(m{\cdot}^\circ C)^{-1}}$), ρ_{blood} is the density of blood in the cervix tissue ($\mathrm{1070\ kg{\cdot}m^{-3}}$), C_{blood} is the blood's specific heat capacity ($\mathrm{4000\ J{\cdot}(kg{\cdot}K)^{-1}}$), ω_{blood} is the blood perfusion rate ($\mathrm{s^{-1}}$), T_{blood} is the cervix's temperature (36 °C), T is the final temperature of the heated up cervix, and Q_{cervix} is the power dissipation density in the cervix ($\mathrm{W{\cdot}m^{-3}}$), which was assumed to be equal to the resistive heat generated by the electromagnetic field according to the equation

$$Q_{\mathrm{cervix}} = \frac{1}{2}\mathrm{Re}[(\sigma - j\omega\varepsilon)E{\cdot}E^*], \quad (6)$$

where σ is the electrical conductivity ($\mathrm{S{\cdot}m^{-1}}$) and ε is the permittivity of the cervix tissue depending on the frequency of microwave radiation computed by using the database available from the Foundation for Research on Information Technologies in Society (FRITS) (Switzerland) (more details in Supporting Information Table S1).

In this model, the electrical field strength and power flow dissipation density values were computed considering the electrical conductivity of free ibuprofen, ≪Ibu-Ag≫ NPs with about 30 nm average diameter in the range from 80 to 8×10^{-4} $\mathrm{S{\cdot}m^{-1}}$, and ≪Ibu-Ag-NrGO≫ NPs with ∼15 nm diameter in the range from 0.8 to 8×10^{-5} $\mathrm{S{\cdot}m^{-1}}$. The values of other parameters were the following: the density of water was 997 $\mathrm{kg{\cdot}m^{-3}}$ and that of ethanol was 789 $\mathrm{kg{\cdot}m^{-3}}$, the specific heat capacity of water was 4187 $\mathrm{J{\cdot}(kg{\cdot}K)^{-1}}$, the density of the cervix tissue was 1105 $\mathrm{kg{\cdot}m^{-3}}$, and its heat capacity at constant pressure was 3676 $\mathrm{J{\cdot}(kg{\cdot}^\circ C)}$.

2.2. Characterization. The synthesized materials were characterized by using the following methods: scanning electron microscopy (SEM) and energy dispersive X-ray (EDX) fluorescence, UV−visible absorption spectroscopy, and Raman microscopy. The morphology and elemental composition of sonochemically prepared NPs were analyzed and characterized by SEM (S-4800, Hitachi, Japan). The UV−visible absorption spectra of colloidal solutions were recorded by using a Cary-500 spectrophotometer (Varian, USA) in the wavelength range from 200 to 1100 nm. For measurements, aqueous solutions were placed in a quartz (SUPRASIL) cuvette (Hellma Analytics 111-QS, Z600725) with a path length of 10 mm. Raman spectra were recorded by using a 3D scanning laser confocal Raman microscope (Confotec NR500, SOL Instruments Ltd., Republic of Belarus) at 473 nm excitation wavelength. The Si wafer with the characteristic Raman line at 520 $\mathrm{cm^{-1}}$ was taken as a reference for calibration and basic alignment during integration time from 1 to 3 s. A linearly polarized diode laser beam was focused through the objectives with 40 and 100× magnification for Raman spectra acquisition. The laser power (≤4 mW) was attenuated by using neutral density filters with the following optical density (OD) values: 0.6 (25), 0.3 (50), and no filter (100).

3. RESULTS AND DISCUSSION

In our design of the nanoplatform, it is hypothesized that ultrasonic complexation of pristine ibuprofen with silver on the surface of ≪NrGO≫ may enhance the acceleration rate of electron transfer processes, thereby activating drug molecules. First, we examine the electronic molecular structure of ultrasonically prepared ≪Ag-NrGO≫ nanoplatform before and after complexation with pristine ibuprofen. Next, the redox reaction of charge transfer between hexacyanoferrate and thiosulfate ions is examined at the contact with ibuprofen complexed with ≪Ag-NrGO≫ in comparison with pristine drug molecules and silver−ibuprofen NPs. The certainty of the hypothesis of pristine drug activation due to the complexation with ≪Ag-NrGO≫ nanoplatform is demonstrated in Scheme 1.

3.1. Molecular Structure of the Platform Based on Nitrogen-Doped rGO Decorated with Silver. First, we prepared N-doped oxidized graphene (≪NrGO≫) as thin flat sheets with an average size of 200 ± 50 nm (Figure S1). The EDX spectrum of ≪NrGO≫ demonstrates distinct peaks of C (60.5 ± 5.8 at. %), O (26.0 ± 3.5 at. %), and N (9.8 ± 1.4 at. %) with an atomic C/O ratio of ∼2.33, indicating the efficient doping of the oxidized graphene structure with nitrogen (Table S2). The produced ≪NrGO≫ also contained some sulfur (3.6 ± 0.3 at. %). Next, ≪NrGO≫ was modified with silver to prepare the ≪Ag-NrGO≫ nanoplatform for ultrasonic complexation with pristine ibuprofen. The structure of ≪NrGO≫ changed by varying the Ag^+ concentration in the aqueous reaction solution: at a small amount of precursor ions, the morphology transforms into rough gray thin sheets of ≪Ag-NrGO≫ with a lateral size of ∼50 ± 10 nm (Figure S2A); at a higher silver ion concentration, it acquires bright spots of spherical shape with an average size of 11.69 ± 2.64 nm (Figure 1 A,B and Figure S2B).

The EDX spectra of these two types of ≪Ag-NrGO≫ are shown in Figure S2, and the elemental composition of NPs is listed in Tables S3 and S4. Analysis of EDX spectra reveals that ≪Ag-NrGO≫ with a rough topology has an atomic C/O ratio ∼2.62 that is higher than in ≪NrGO≫ (∼2.33) because the

https://doi.org/10.1021/acsbiomaterials.2c01045
ACS Biomater. Sci. Eng. XXXX, XXX, XXX−XXX

Scheme 1. Schematic Illustration Demonstrates the Principle of Pristine Ibuprofen Activation by Ultrasonic Complexation (20 kHz) with the Silver Modified Nitrogen-Doped Oxidized Graphene (≪Ag-NrGO≫) Nanoplatform[a]

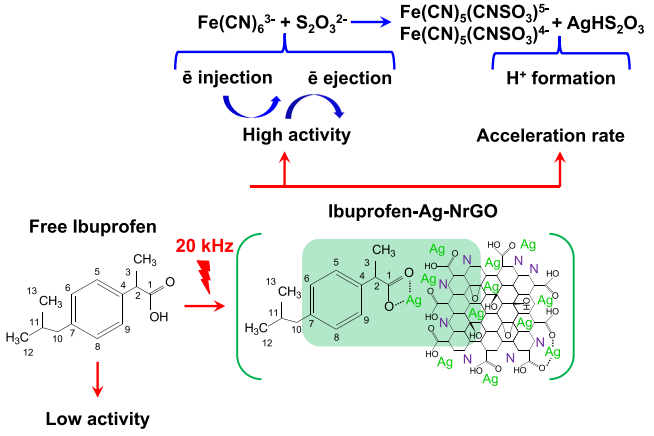

[a]Free ibuprofen exhibits a ∼42 times lower catalytic activity of the electron transfer in the reaction of hexacyanoferrate and thiosulfate ions than ≪Ibu-Ag-NrGO≫ nanoparticles. The higher activity of ≪Ibu-Ag-NrGO≫ can be explained by the injection/ejection of electrons by semiconducting organic molecular crystals of ibuprofen at the contact with ≪Ag-NrGO≫ due to increased electron density, specific bond formation between the carboxylic groups, and Ag, Ag-cluster structure in N-doped ordered carbon lattice and H-bonds. The enhanced acceleration reaction rate can be attributed to the excess production of H^+ resulting in the formation of intermediate reaction species $Fe(CN)_5(CNSO_3)^{x-}$ (x = 4 or 5) and $AgHS_2O_3$, which increase the oxidation action of $Fe(CN)_6^{3-}$ ions.

nitrogen-doped oxidized graphene structure was decorated with silver through replacement of oxygen according to the higher atomic concentration of N (∼11.7 at. %) and S (∼5.6 at. %) and a lower amount of O (∼22.5 at. %) in comparison with ≪NrGO≫ (O ∼26.0 at. %). For comparison, in the second type of ≪Ag-NrGO≫ with bright nanospheres, the atomic concentration of silver increased 3.5 times, but the amount of nitrogen and sulfur decreased ∼3.3 and ∼1.7 times, and the atomic C/O ratio decreased to ∼2.1, indicating the contribution of oxygen groups in PEG molecules to the reduction and stabilization of spherical Ag nanostructures on the surface of ≪NrGO≫. Overall, in contrast to oxygen, the atomic concentration of C in NPs was almost the same: in ≪NrGO≫, it was ∼60.5 at. %, and in ≪Ag-NrGO≫ with a lower and higher concentration of silver, it was ∼59.0 and ∼60.1 at. %, meaning that ultrasonic doping of the as-synthesized ≪rGO≫ structure was nondestructive to the carbon lattice. For comparison, the EDX analysis of ≪Ag-NrGO≫ NPs after complexation with ibuprofen *per se* revealed the following atomic concentrations of elements (in at. %): C = 55.2 ± 2.8, O = 17.4 ± 1.3, S = 9.2 ± 0.4, N = 8.4 ± 0.7, and Ag = 8.2 ± 1.1, demonstrating that the C atom concentration was lower on ∼5 at. % than in the ≪Ag-NrGO≫ nanoplatform (Figure S3).

Raman spectra of ≪NrGO≫ and ≪Ag-NrGO≫ NPs are shown in Figure 1C. The Raman spectrum of ≪NrGO≫ reveals two strong peaks at ∼1354 cm^{-1} (D band) and ∼1586 cm^{-1} (G band).[55] The appearance of the D vibrational band is caused by a disordered carbon nanostructure,[56] and its peak position indicates GO in its reduced form[57] and a diamond-like arrangement of carbon atoms.[58] The D band of ≪NrGO≫ has a FWHM magnitude ∼194 cm^{-1} and a lower intensity (∼4775) in comparison with the G band

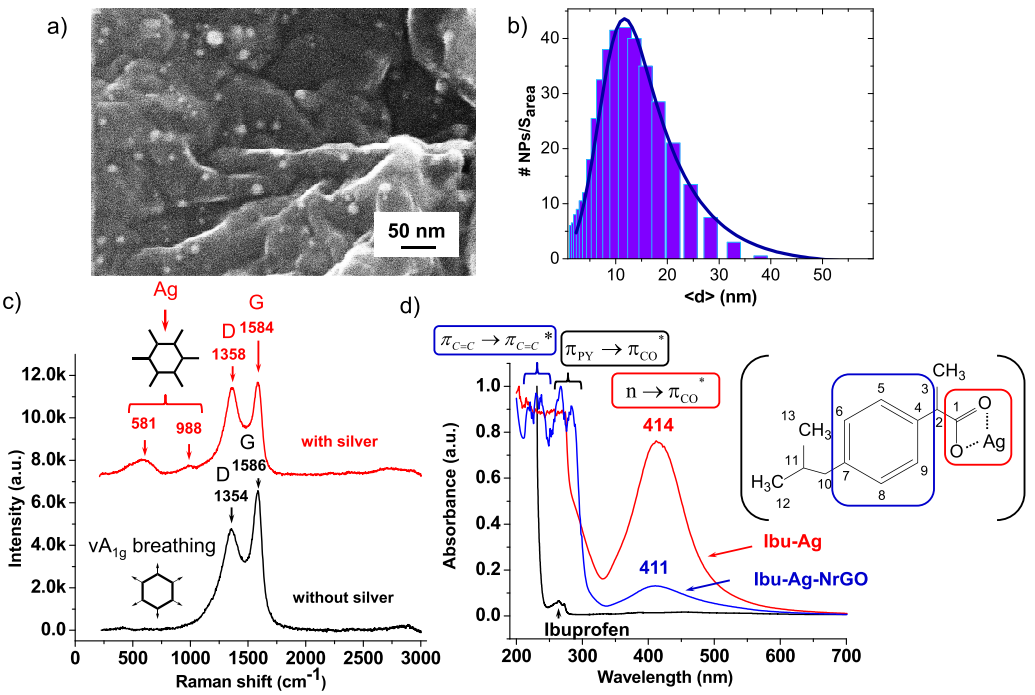

Figure 1. (A) A representative SEM image of synthesized ≪Ag-NrGO≫ nanoparticles is shown. (B) The size distribution histogram (number of NPs per surface area versus the average size <*d*>, nm) of ≪Ag-NrGO≫ nanoparticles is demonstrated. (C) Raman spectra of prepared ≪NrGO≫ (black) and ≪Ag-NrGO≫ (red) at λ_{exc} = 473 nm are presented. (D) UV−vis absorption spectra of aqueous solutions (pH 5.5) containing synthesized ≪Ibu-Ag≫ and ≪Ibu-Ag-NrGO≫ nanoparticles in comparison with pristine ibuprofen are displayed.

https://doi.org/10.1021/acsbiomaterials.2c01045
ACS Biomater. Sci. Eng. XXXX, XXX, XXX−XXX

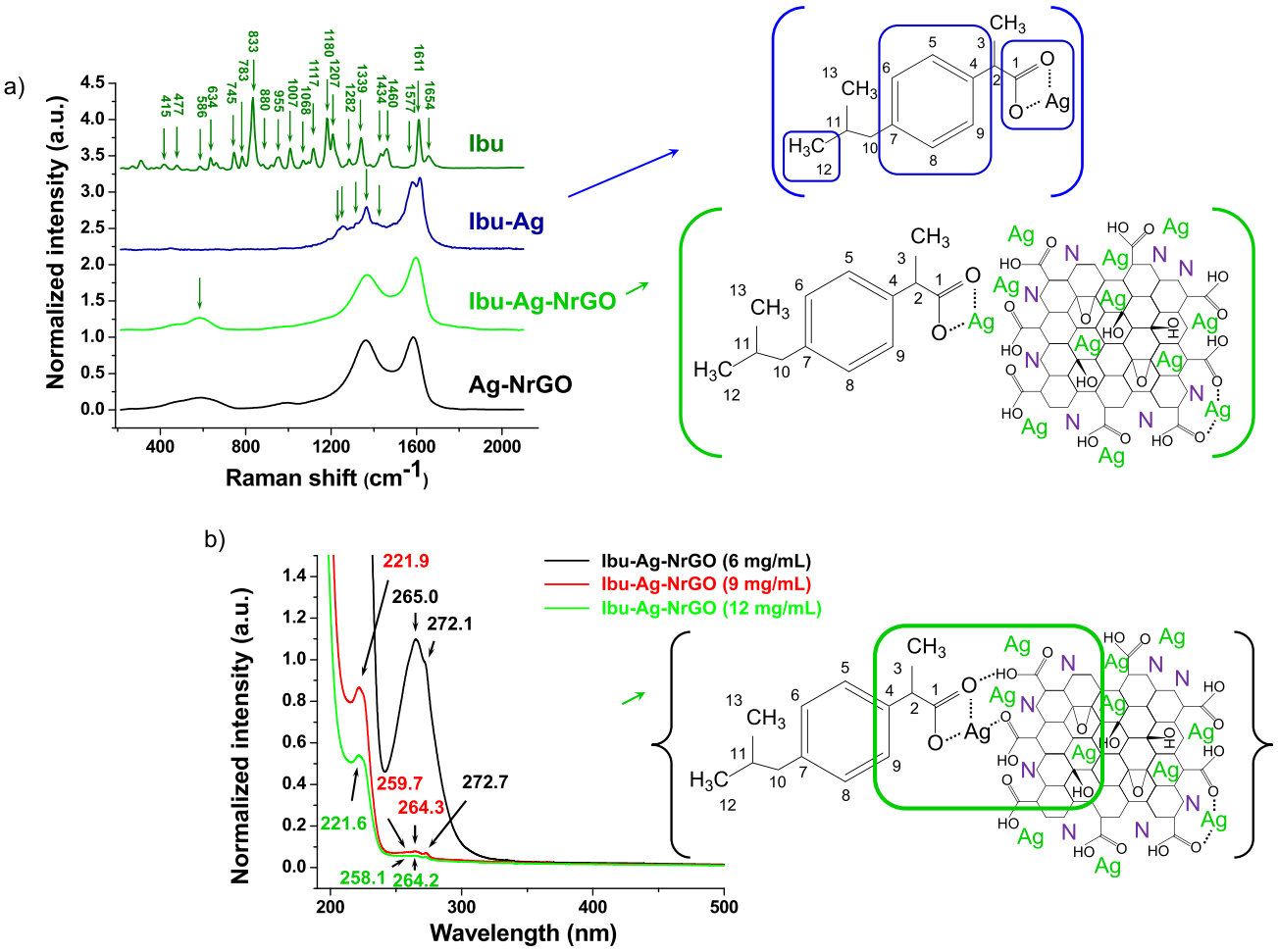

Figure 2. (A) Raman spectra of synthesized ≪Ibu-Ag≫ and ≪Ibu-Ag-NrGO≫ nanoparticles in comparison with pristine ibuprofen (Ibu) (λ_{exc} = 473 nm) are shown. The inset shows a deduced molecular structure of formed ≪Ibu-Ag≫ nanoparticles before and after interaction with the ≪NrGO≫ platform. (B) UV−vis absorbance spectra of aqueous solutions of formed ≪Ibu-Ag-NrGO≫ nanoparticles at concentrations from 6 to 12 mg/mL are shown. The inset indicates the deduced molecular structure of ≪Ibu-Ag-NrGO≫ nanoparticles at a concentration of 6 mg/mL.

(FWHM ∼103 cm^{-1}, ∼6585), and the intensity IntD/IntG ratio is ∼0.73. The broadening and weakening of the D band in ≪NrGO≫ may occur owing to the recovery of zones of carbon atoms with sp^2-hybridization that is caused by the formation of defects, vacancies, and distortions in oxidation and doping of carbon lattice by nitrogen.

Distinct from ≪NrGO≫, in the Raman spectrum of ≪Ag-NrGO≫, small peaks at ∼581 and ∼988 cm^{-1} indicate the formation of a Ag complex with the carbon phenyl ring (Figure 1C). The vibrational mode at ∼581 cm^{-1} can be assigned to the twisting of the hydroxyl group surrounded by nitrogen atoms[59] and to (HO)-NO_2 vibrations. The peak at ∼988 cm^{-1} can arise due to C−H vibrations of pyridine coordinated with silver through the nitrogen atom and hydrogen bonds formed with water molecules.[60] Pyridine can be separated by a monolayer of water molecules being oriented in a high electric field as experimentally confirmed by the relationship between the change in the wavenumber of this band and the electrical potential.

The upshift of the D band in ≪Ag-NrGO≫ at ∼1358 cm^{-1} can be caused by the formation of single grain crystals in well-crystallized graphite phase[61] and by the higher sensitivity of these NPs to the laser irradiation in contrast to ≪NrGO≫. It can be assumed that small aromatic clusters are formed in ≪Ag-NrGO≫ because they have increased vibrational modes, resulting in a shift of the D band to higher wavenumbers. In this regard, aromatic clusters can be ordered because the D band of ≪Ag-NrGO≫ becomes narrower (∼145 cm^{-1}) than that of ≪NrGO≫ (∼194 cm^{-1}). On the other hand, the G band in ≪Ag-NrGO≫ position is shifted at ∼1584 cm^{-1}, demonstrating an increased concentration of carbon atoms with sp^2-hybridization with a decreased number of carbon layers. The downshift of the G band indicates that oxidation of ≪NrGO≫ does not occur. Consequently, a lower C/O ratio (∼2.1) can be caused by the formation of a complex ≪Ag-NrGO≫ structure with PEG due to interaction with oxygen-containing groups. It is important to note that the FWHM value of the G band of ≪Ag-NrGO≫ (∼103 cm^{-1}) is comparable to that of ≪NrGO≫ (∼103 cm^{-1}), revealing the formation of nanocrystallites with a graphite phase in an ordered structure of carbon sheets in the process of silver reduction. In contrast to ≪NrGO≫, the IntD/IntG (4074/4333) ratio of ≪Ag-NrGO≫ is ∼0.94 as a result of the less elastic light scattering, indicating the smaller crystallite size of carbon zones with sp^2-hybridization than that in ≪NrGO≫.

3.2. Surface Electronic Structure of Complexed Pristine Ibuprofen with Silver NrGO. Ultrasound (20 kHz) irradiation was applied to the ≪Ag-NrGO≫ nanoplatform to form complexes with pristine ibuprofen in an aqueous medium. Control experiments were carried out with only silver

https://doi.org/10.1021/acsbiomaterials.2c01045
ACS Biomater. Sci. Eng. XXXX, XXX, XXX−XXX

to find out the role of ≪NrGO≫ in the electronic structure of ≪Ag-NrGO≫. The complex formation of pristine ibuprofen with silver in an aqueous ≪NrGO≫ solution was examined by using the method of absorption spectrophotometry.

The UV−vis absorbance spectra of aqueous solutions of pristine ibuprofen, ≪Ibu-Ag≫, and ≪Ibu-Ag-NrGO≫ NPs are shown in Figure 1D. Pristine ibuprofen in aqueous ethanol solution (30 wt %, pH = 5.5) exhibits a broad absorption peak with three maxima at ∼257.3, 264.5, and 272.7 nm. The absorption peak at 257.3 nm corresponds to the hydroxylated products in the phenyl ring during its reaction with hydroxyl $^{\bullet}$OH radicals, as a result of which the transition hydroxycyclohexadienyl radical is converted into a hydroxylated molecule. The other two absorption peaks at ∼264.5 and 272.7 nm indicate changes in the electronic molecular structure of phenyl molecules in the formation of benzyl-type radicals without substitution in the side chain.[62] Three absorption maxima can be attributed to the electronic transitions of ibuprofen, $\pi_{PY} \rightarrow \pi_{CO}^*$, occurring between the phenyl ring and C−O bonds caused by oxidation of hydroxyl radicals.

Unlike pristine ibuprofen, the absorption spectrum of an aqueous solution of ≪Ibu-Ag≫ shows several weakly resolved peaks in the high-energy region (∼210−215, ∼215−273 nm) and a strong broad band with a maximum at ∼414 nm. Peaks in the region of 210−215 nm can be attributed to the electronic $n-\pi^*$ transitions in the carboxyl group of ibuprofen, and those in 215−273 nm can be attributed to the electronic $\pi-\pi^*$ transitions of its modified phenyl group. A strong absorption band shows the $n-\pi_{CO}^*$ electronic transition in the entire structure of NPs, which occurs during the charge transfer between ibuprofen molecules having C−O bonds in a complex with silver.

When comparing the absorption spectra of ≪Ibu-Ag≫ and ≪Ibu-Ag-NrGO≫, it can be noticed that, in the latter, a bathochromic shift of the band appears from 414 to 411 nm. The weakening of this band is accompanied by an increase in electronic $\pi_{C=C} \rightarrow \pi_{C=C}^*$ transitions in the altered phenyl ring and $\pi_{PY} \rightarrow \pi_{CO}^*$ in ibuprofen occurring between the phenyl ring and C−O bonds as a result of the interaction with hydroxyl radicals. Because the bathochromic shift is caused by groups acting as electron donors, it can be assumed that the absorption of such donor molecules leads to an increase in the electron density of ≪Ibu-Ag-NrGO≫. Therefore, it can be concluded that the carboxyl group of ibuprofen is directly involved in the complex formation with silver. As a consequence, there is an increase in the electron density of ≪Ibu-Ag-NrGO≫ due to interaction with the oxidized form of the phenyl group.

The surface electronic structure of ≪Ibu-Ag-NrGO≫ was further assessed by Raman spectroscopy (Figure 2A). To understand its structure in more details, Raman spectra of pristine ibuprofen and the ≪Ag-NrGO≫ nanoplatform are shown. A detailed description of characteristic vibrational lines of pristine ibuprofen is given in Table S5. Among numerous vibrational bands, the peak at ∼745.9 cm^{-1} is the characteristic peak of ibuprofen, indicating the degree of purity of its co-crystal.[63] The peak at ∼1460.5 cm^{-1} is caused by the characteristic vibration of the hydrogen bond between carboxylate groups and water molecules of ibuprofen. The vibrational band at ∼1340 cm^{-1} of pristine drug molecule does not split, indicating that ibuprofen has an ordered structure in phase I with δ, that is, the difference between $\nu_{asym}(COO-)$ at ∼1587 cm^{-1} and $\nu_{sym}(COO-)$ at ∼1405 cm^{-1} being ∼182 cm^{-1}.

The Raman spectra of ≪Ibu-Ag≫ and ≪Ibu-Ag-NrGO≫ NPs differ from the spectrum of the pristine ibuprofen by a reduced number of vibrational bands and their noticeable broadening accompanied by a shift (Figure 2A, Tables S6 and S7). In the spectra of ≪Ibu-Ag-NrGO≫, the vibrational band ν(C−O) of the carboxyl group is upshifted by 27 cm^{-1}, but symmetric $\nu_{sym}(COO^-)$ and asymmetric $\nu_{asym}(COO^-)$ vibrational bands are downshifted by ∼8 and ∼7 cm^{-1} because of the complexation of ibuprofen with silver and ≪NrGO≫. The C−C stretching, CH_2 twist, and C−C−H deformation are upshifted by 5 cm^{-1} in ≪Ibu-Ag-NrGO≫. The δ value (between peaks at 1445 and 1579 cm^{-1}) in these nanoparticles is 134 cm^{-1}, which is less than that in pristine ibuprofen (182 cm^{-1}) and is in a good agreement with the literature data of ibuprofen−silver complexes (127 cm^{-1}).[64] The Raman peaks of in-plane CH phenyl ring deformation and bending are upshifted by 6 cm^{-1} because of the formation of hydrogen bonds between carboxylate groups and water molecules.

The Raman spectra of ≪Ibu-Ag-NrGO≫ and ≪Ag-NrGO≫ show the systematic appearance of active vibrational modes of the silver-aromatic complex with characteristic peaks at ∼584, ∼992 and ∼593, ∼995 cm^{-1}, but the deformation vibrational bands appear only in ≪Ibu-Ag-NrGO≫ (Table S7). The D vibrational band is similar to ≪Ibu-Ag-NrGO≫ and ≪Ag-NrGO≫, in contrast to the G mode, which is upshifted by 11 cm^{-1} in ≪Ibu-Ag-NrGO≫. The G vibrational band of ≪Ibu-Ag-NrGO≫ at ∼1597 cm^{-1} is a complex vibration consisting of in-plane deformation modes of C1C6 and CH phenyl ring of ibuprofen and C−C stretching.

Next, let us consider the UV−vis absorption spectra of ≪Ibu-Ag-NrGO≫ stabilized by PEG at concentrations of NPs from 6 to 12 mg/mL (pH 5.5) (Figure 2B). A distinctive feature of these spectra is the appearance of a characteristic triplet maximum of ibuprofen in the region of 258−272 nm and of an ≪NrGO≫ peak at ∼221 nm. At a concentration of 6 mg/mL, the absorption peak of ibuprofen appears with maxima at ∼222−225 and 265 nm and a weak shoulder at ∼272 nm caused by the electronic $\pi-\pi^*$ transitions in the phenyl ring of ibuprofen, ≪NrGO≫, and ibuprofen−Ag complexes.[65] Because the characteristic absorption peaks of ≪NrGO≫ did not appear at 237, 242, or 296 nm, it can be concluded that ≪NrGO≫ forms a complex with silver and ibuprofen. Therefore, absorption peaks appear as a result of $\pi-\pi^*$ electronic transitions in the phenyl ring of ibuprofen in complex with silver atoms. Moreover, the absorption peak intensity is directly proportional to the concentration of bound silver atoms. Comparing the intensities of these peaks, we can conclude that a greater number of silver atoms are formed in silver−graphene complexes with ibuprofen at a concentration of 9 mg/mL.

Another important feature is the absence of a characteristic surface plasmon resonance peak of silver NPs and their individual complexes with ibuprofen, in contrast to ≪Ibu-Ag-NrGO≫ at 3 mg/mL in Figure 1D. Therefore, at an increased concentration of ≪NrGO≫, ultrasonic complexation of ibuprofen with silver does not lead to the growth of silver nanoparticles on the surface of ≪NrGO≫ but leads to the formation of an atomic silver cluster structure in a complex with ibuprofen.

It should be noted that ultrasonic activation of silver−graphene complexes of ibuprofen with PEG not only leads to

https://doi.org/10.1021/acsbiomaterials.2c01045
ACS Biomater. Sci. Eng. XXXX, XXX, XXX−XXX

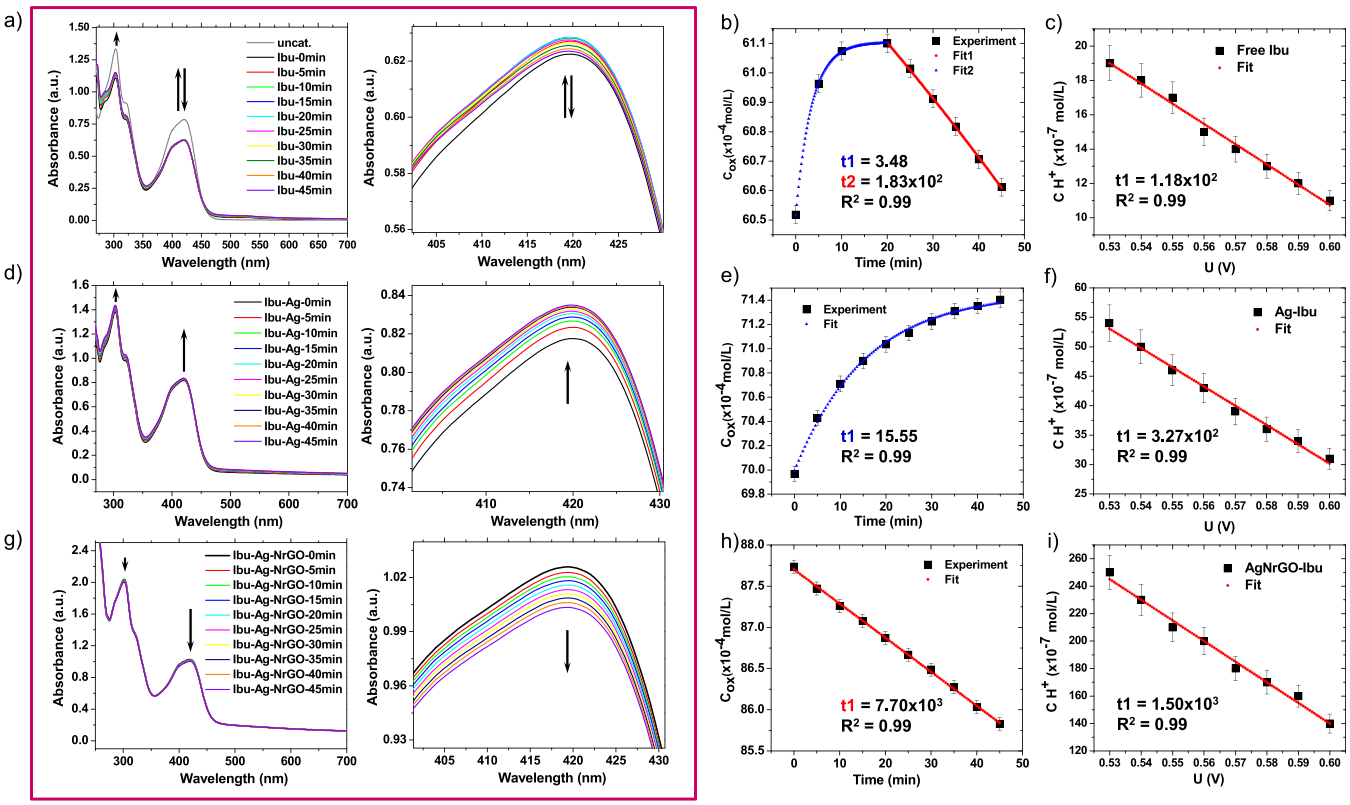

Figure 3. (A, D, G) UV−vis absorption spectra of aqueous solutions of 200 μL of 0.01 M $Fe(CN)_6^{3-}$ and 200 μL of 0.1 M $S_2O_3^{2-}$ with pristine ibuprofen (5 mM, 30 wt %), ≪Ibu-Ag≫, and ≪Ibu-Ag-NrGO≫ nanoparticles during 45 min of reaction with a local zoom-in peak near 420 nm are shown. (B, E, H) The plots show the dependence of the absorption intensity peak at 420 nm on the concentration of $Fe(CN)_6^{3-}$ (C_{ox}(×10^{-4} mol/L)) (black dots). (B) The experimental data of C_{ox}(×10^{-4} mol/L) in the aqueous solution with pristine ibuprofen are fitted to the exponential functions $y = 61 - 0.59\exp(x/-3.48)$ during the first 20 min (red dots) and $y = 65 - 3.02\exp(x/-183.25)$ during the next 25 min (blue dots) with a Pearson's correlation coefficient $R^2 = 0.99$. (E) The experimental data of C_{ox}(×10^{-4} mol/L) in the aqueous solution with ≪Ibu-Ag≫ are fitted to the exponential function $y = 72 - 1.47\exp(x/-15.55)$ during 45 min of reaction (blue dots) with a Pearson's correlation coefficient $R^2 = 0.99$. (H) The experimental data of C_{ox}(×10^{-4} mol/L) in the aqueous solution with ≪Ibu-Ag-NrGO≫ are fitted to the exponential function $y = -232 + 319.16\exp(x/-7696.85)$ during 45 min of reaction (red dots) with a Pearson's correlation coefficient $R^2 = 0.99$.

an increase in the intensity of the absorption band of ibuprofen but also causes changes in the band at 265 nm in the short-wavelength region of the spectrum. Changes of the latter band can be caused by the intramolecular interaction of PEG with ibuprofen. In this regard, an increase in the solubility of ibuprofen in an aqueous solution of PEG indicates the formation of a complex of these two substances. It is also important to note that the absorption bands of the phenyl ring of ibuprofen are broadened due to the group bending C−C−H vibrations. Further changes in the absorption bands may be caused by electronic transitions in the phenyl ring and indicate an intermolecular interaction between PEG and ibuprofen. It is unlikely that the formation of a weak hydrogen bond between the carboxyl group of ibuprofen and the hydroxyl or ester group of PEG leads to changes in the electronic structure of the phenyl ring. Presumably, the interaction of ibuprofen with PEG is predominantly transconformational.[66]

Overall, one can conclude that the process of charge transfer between ibuprofen molecules with silver can occur through C−O bonds in carboxyl and phenyl groups. In ≪Ibu-Ag-NrGO≫, electron density can be increased because the carboxyl group of ibuprofen is directly involved in complex formation with silver and the oxidized form of phenyl group. In ≪Ibu-Ag-NrGO≫, ≪NrGO≫ is found only in a complex with an atomic-cluster structure of silver and ibuprofen, and more silver atoms are formed in silver−graphene complexes with ibuprofen at a nanoparticle concentration of 9 mg/mL. During the complexation of silver with the carboxyl group of ibuprofen, hydrogen bonds are formed between the carboxyl groups of ≪Ibu-Ag≫ and ≪Ibu-Ag-NrGO≫ NPs and water molecules.

3.3. Electrokinetic Efficiency of ≪Ibu-Ag-NrGO≫. The electrokinetic activity of ≪Ibu-Ag-NrGO≫ was assessed in an oxidation of thiosulfate $S_2O_3^{2-}$ by hexacyanoferrate(III) $Fe(CN)_6^{3-}$ ions in aqueous colloidal solutions at room temperature. The electron transfer process was studied at a molar concentration ratio of $[Fe(CN)_6^{3-}]$ to $[S_2O_3^{2-}]$ of 1:10 at pH 5.5 by recording the UV−vis absorbance spectra with the time interval of 5 min during 45 min of the reaction period (Figure 3). At the beginning, an aqueous solution of 200 μL of 0.01 M $Fe(CN)_6^{3-}$ and 200 μL of 0.1 M $S_2O_3^{2-}$ had a yellow color and exhibited three distinct peaks at 246 nm (~40,650.41 cm^{-1}), 303 (~33,003.30 cm^{-1}) with a shoulder at 320 nm (~31,250.00 cm^{-1}) and 420 nm (~23,809.52 cm^{-1}) (Figure S4A). The first absorption peak indicates charge transfer in d^6 ferricyanide being attributed to an L → M process.[66] The absorption maximum at 303 nm with a shoulder can be assigned to $Fe^{3+}(H_2O)_6HO_2^-$ with several inner-sphere complexes of d^5 ferric ion with the ground-state configuration $(3t_{1u})^6(2t_{2g})^5 = {}^2T_{2g}$, indicating parity-allowed g → u (intense band) with d → d (shoulder) transitions as a result of their proximity to intense bands. The broad

https://doi.org/10.1021/acsbiomaterials.2c01045
ACS Biomater. Sci. Eng. XXXX, XXX, XXX−XXX

absorption band at ~420 nm can be assigned to one of the Laporte-allowed transitions of L → M type arising as a result of electron excitation from the $3t_{1u}$ into the $2t_{2g}$ level of the d^5 ferrocyanide ion complexes.

The course of the reaction was followed by monitoring the decrease in the absorbance of hexacyanoferrate(III), continuously as a function of time, at 420 nm. After 45 min of this process, the solution did not become colorless, indicating that the final reaction products such as $Fe(CN)_6^{4-}$ and SO_4^{2-} ions were not formed because of the excess of the initial concentration of thiosulfate ions. In the absence of a catalyst at a fixed concentration of $S_2O_3^{2-}$, the intensity of the absorption peak at 420 nm has a linear relationship with the concentration of $Fe(CN)_6^{3-}$ ions in the range from 0.001 to 0.01 mol/L, which was used as a calibration plot (Figure S4B). In general, the initial rate of reaction is independent of the amount of $Fe(CN)_6^{3-}$ ions, and 0.01 M concentration was used for the study. The redox exchange ferricyanide−ferrocyanide ions' reaction does not take place in the aqueous solution with thiosulfate ions without a catalyst (Figure S4).

In the presence of pristine ibuprofen (5 mM, 30 wt %), the UV−vis absorption spectra of the reaction solution showed a small peak at 272 nm (~36,764.71 cm^{-1}), a distinct maximum at 303 nm (~33,003.30 cm^{-1}) with two shoulders at 283 (~35,335.69 cm^{-1}) and 321 nm (~31,152.65 cm^{-1}), and a peak at 420 nm (~23,809.52 cm^{-1}) (Figure 3A). The first absorption band can be assigned to the complex of ibuprofen with d^5 ferrocyanide ions with d → d transitions involving charge-transfer processes in phenyl molecules without substituted side chains. The other two intense absorption bands indicate $^2T_{2g}$ electronic transitions of ferrocyanide ion complexes with spin-allowed d → d transitions. The slightly downshifted shoulder at 31,152.65 cm^{-1} reflects the deprotonation of the nitrogen end of cyanide as evidenced in the ethanol solution of ferrocyanide ions by the shift of the first d → d transition from 31,000 cm^{-1}, indicating increased back-bonding in the deprotonated species resulting from destabilization of the t_{2g} level. After 45 min of reaction, the intensities of small peaks increased in the range from 250 to 321 nm (Figure S5A), but not the analytical peak at 420 nm, indicating the increased electron density of ibuprofen−ferrocyanide complexes.

However, during the first 20 min of this reaction, the intensity of the band at 420 nm increased at a reaction rate ~3.48, but during the next 25 min, it decreased at a reaction rate ~183.25 (Figure 3B). The slow exchange reaction of ferrocyanide−ferricyanide ions can occur by a one-electron process involving positive ions, but the negative charges cannot be excluded as evidenced by the accelerated exchange rate after 25 min. Therefore, the positive ion presumably would be present as aquo-complexes or at least as highly hydrated species and would present an external sheath mainly of hydrogen atoms because the oxygen atoms in the water molecules should be oriented toward the metal ions. Indeed, the charge transfer on the surface of pristine ibuprofen is mediated by H-bonds involving phenyl groups between carboxylate groups and water molecules, providing peripheral H atoms bearing a positive formal charge and leading to the retention of electrokinetic efficacy of ibuprofen during the first 20 min of reaction. These peripheral hydrogens would be expected to bear a positive formal charge, and this electron deficiency would reduce the chance of electron exchange on collision between two such ions. As the mechanism of kinetics of oxidation of thiosulfate by hexacyanoferrate(III) in aqueous alkaline media can be interpreted in terms of a spontaneous change of thiosulfate in a rate-determining step followed by a rapid reduction of hexacyanoferrate(III), the slow step can arise as a result of the formation of a bond to sulfur, which will require activation energy. On the other hand, the external nitrogen atoms in the ibuprofen−cyanide complexes bear a negative formal charge, and the central ion is thus surrounded by a sheath of electron-rich atoms; this higher electron density may accelerate the rapid exchange. In our solution with pristine ibuprofen, the initial increase of the absorption intensity at 420 nm can occur as a result of the increased H^+ concentration at the contact with ibuprofen during the first 20 min of reaction, which can lead to the formation of ion pair Ibu-$Fe(CN)_6^{3-}$ and $HFe(CN)_6^{3-}$, being regarded as the active oxidant that can contribute to the oxidation of ibuprofen and thiosulfate ions, resulting in the acceleration of this reaction during the next 25 min. In addition, electronic transitions of ibuprofen between the phenyl ring and C−O bonds caused by oxidation can lead to an enhanced efficacy of ibuprofen. In particular, $Fe(CN)_6^{3-}$ reacts with H^+, resulting in $HFe(CN)_6^{2-}$, which also reacts with $S_2O_3^{2-}$ and leads to the formation of $S_2O_3^-$ and $HFe(CN)_6^{3-}$, and this reaction is slow. In addition, $S_2O_3^-$ can react with H^+, resulting in the formation of $S_4O_6^{2-}$, but at a faster rate. The $S_4O_6^{2-}$ ions undergo subsequent disproportion to $S_3O_6^{2-}$ and $S_2O_3^{2-}$ on long standing. This is in agreement with the increased intensities of absorption peaks in the range from 272 to 321 nm. Therefore, the role of H atom and hydrogen bonds between carboxylate groups and water molecules of ibuprofen is crucial to the reaction.

The UV−vis absorption spectra of ≪Ibu-Ag≫ show two intense bands at ~302 (33,112.58 cm^{-1}) with the shoulders at 285 (35,087.72 cm^{-1}) and 322 nm (31,055.90 cm^{-1}) and at ~421 nm (23,752.97 cm^{-1}) (Figure 3D). In contrast to pristine ibuprofen (~3.48), the absorption intensities of all peaks were increased during 45 min of reaction at a 4.5 times faster rate (~15.55) as estimated from the exponential fit function (Figure 3E and Figure S5B). In addition, in ≪Ibu-Ag≫, the main peaks and their shoulders exhibited a bathochromic shift of 1−2 nm, and the concentration of oxidant ions in this process was higher at 10.3 (~71.4) in comparison with pristine ibuprofen (~61.1). Distinct from pristine ibuprofen, ≪Ibu-Ag≫ has a silver−aromatic complex and enhanced electronic transitions in the entire structure of NPs, which lead to acceleration of the charge transfer between the phenyl and carboxyl groups of ibuprofen molecules in a complex with Ag having C−O bonds. The electron exchange mechanism in ≪Ibu-Ag≫ resembles that in pristine ibuprofen during the first 20 min of exchange reaction between $Fe(CN)_6^{3-}$ and $S_2O_3^{2-}$ involving H^+, $HFe(CN)_6^{2-}$, and $HFe(CN)_6^{3-}$ but at a faster rate due to the increased electron density of NPs.

Similar to ≪Ibu-Ag≫, the UV−vis absorption spectra of ≪Ibu-Ag-NrGO≫ show absorption maxima at ~302 (33,112.58 cm^{-1}) and ~421 nm (23,752.97 cm^{-1}) but with one shoulder at 322 nm (31,055.90 cm^{-1}), with decreased intensities during 45 min of reaction (Figure 3G and Figure S5C). The concentration of oxidant ions decayed from ~87.7 × 10^{-4} mol/L at the beginning of reaction to ~85.8 × 10^{-4} mol/L after 45 min at a 42 times faster reaction rate (~7696.85) than pristine ibuprofen (~183.25) (Figure 3H). The enhanced catalytic performance of ≪Ibu-Ag-NrGO≫ NPs is likely to be governed by charge injection/ejection

https://doi.org/10.1021/acsbiomaterials.2c01045
ACS Biomater. Sci. Eng. XXXX, XXX, XXX−XXX

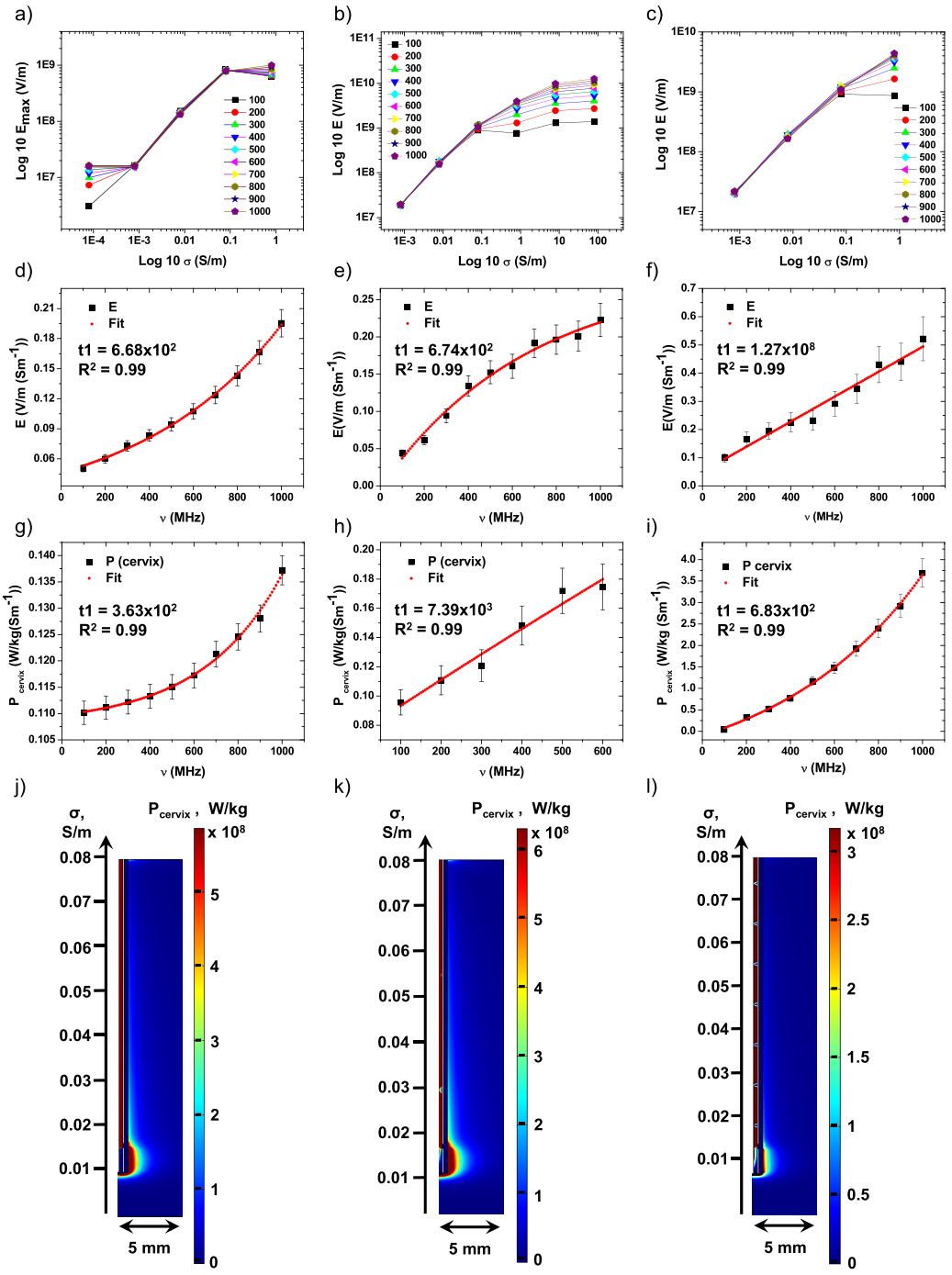

Figure 4. The plots show the dependence of the calculated electric field strength maximal peak values (E_{max}, V/m) on the electrical conductivity (σ, S/m) of (a) pristine ibuprofen, (b) ≪Ibu-Ag≫, and (c) ≪Ibu-Ag-NrGO≫ being on the surface of the electrode inserted into the cervix tumor tissue under microwave irradiation in the frequency range from 100 MHz to 1 GHz. The plots reveal the computed speed of E_{max} magnitude change versus the electrical conductivity (E, V/m(Sm^{-1})) under applied microwave irradiation field inside the cervix tumor tissue with (d) pristine ibuprofen, (e) ≪Ibu-Ag≫, and (f) ≪Ibu-Ag-NrGO≫. The plots demonstrate the computed speed of the total power dissipation density of flow distribution versus the electrical conductivity P_{cervix} (W/kg(Sm^{-1})) and its total power dissipation density magnitudes in the range of σ from 0.01 to 0.08 S/m with the highest values of the electromagnetic field at 100 MHz−1 GHz near the electrode's tip and the slot inside of the cervix tumor tissue with (g, i) pristine ibuprofen, (h, k) ≪Ibu-Ag≫, and (i, l) ≪Ibu-Ag-NrGO≫.

processes into and out of the surface of the individual semiconducting crystals. The overall increased electron density of these NPs due to electronic $\pi_{c=c} \rightarrow \pi_{c=c}^*$ transitions in the altered phenyl ring and $\pi_{py} \rightarrow \pi_{co}^*$ in ibuprofen between the phenyl ring and C−O bonds, groups in ≪NrGO≫ acting as electron donors, and atomic Ag-cluster structure in a ferrocyanide−ibuprofen complex can alleviate the barrier and significantly increase the reaction rate. From kinetic measurements of some phenols, one can conclude that aryloxy radicals can be formed at the contact of $Fe(CN)_6^{3-}$ ions with ≪Ibu-Ag-NrGO≫.[67] As a consequence of this reaction, diaryls or diaryl ethers can be obtained as final products. These reaction products are stable because of the delocalization of the odd electron by resonance, particularly over the ortho and para

https://doi.org/10.1021/acsbiomaterials.2c01045
ACS Biomater. Sci. Eng. XXXX, XXX, XXX−XXX

positions of the aromatic ring. Oxidation of phenols by ferricyanide shows that the dimers may arise from condensations between phenoxy anions and aryloxy cations. This would mean that the coupling process is heterolytic, involving a cationic substitution of the phenol by a mesomeric aryloxy cation formed after a two-step oxidation of the phenoxy radical. Consequently, the increase of the reaction rate is proportional to the increased concentration of the oxidizable species such as aryloxy anions. This is in agreement with the hydrolyzed phenol rings of ≪Ag-NrGO≫ and ibuprofen complexes with a silver cluster structure in ≪Ibu-Ag-NrGO≫ NPs. According to the mechanism proposed for the oxidation of aldehydes, ketones, and nitroparafins, we may suggest that a complex is formed between ferricyanide and the enolate anions of ≪Ibu-Ag-NrGO≫ and possibly between ferricyanide anion and a mesomeric structure of the enolate anion. This complex can be attacked by a second ferricyanide ion, resulting in the formation of final products with increased catalytic activity. On the other hand, thiosulfate ion $(S_2O_3)_2^{3-}$ can form strong silver−thiosulfate complexes $Ag(S_2O_3)_2^{3-}$. The studies of the oxidation kinetics of $S_2O_3^{2-}$ by metallic oxidants prove the formation of precursor metal−thiosulfate complexes in an equilibrium step preceding the electron transfer. Oxidation by transition metal complexes may proceed via intermediate complexes of $Fe(CN)_5(CNSO_3)^{5-}$ and $Fe(CN)_5(CNSO_3)^{4-}$. It has been suggested that in the outer-sphere electron transfer mechanism, the cyanide ligands play a significant role in view of the lower reactivity of the protonated complexes $Fe(CN)_6H^{3-}$ and $Fe(CN)_6H_2^{2-}$ with OH. Therefore, reaction of H^+ with $S_2O_3^{2-}$ and Ag will lead to the formation of the active complex ≪$AgHS_2O_3$≫, and this will accelerate the action of $Fe(CN)_6^{3-}$. The rate of subsequent biomolecular processes with ibuprofen may be high when the concentration of reactants is of the order of 10^{-6}−10^{-4} mol/L, and the activation energy is small. Therefore, it is likely that attack by $Fe(CN)_6^{3-}$ would become rate determining.

To understand the role of ibuprofen and individual inorganic components of ≪Ibu-Ag-NrGO≫, a series of control experiments have been performed in the study of the charge exchange reaction between hexacyanoferrate and thiosulfate ions—≪Ag-NrGO≫, ≪Ag-rGO≫, or 5 mM $AgNO_3$—before and after stabilization with PEG and NPs without Ag (Figures S6−S8). All UV−vis absorption spectra exhibited bands similar to ≪Ibu-Ag-NrGO≫ at 302−303 nm with a shoulder at 322 nm and a characteristic peak at 420 nm but with lower reaction rates. In particular, the reaction rate of PEG-coated ≪Ag-NrGO≫ was ∼157.61 and that of ≪NrGO≫ was ∼66.80, demonstrating the important role of Ag in catalysis (Figure S6). Absorption spectra of the charge exchange reaction between free Ag cations and those in the PEG matrix revealed comparable reaction rates of ∼32.02 and ∼34.75, indicating that PEG acts as a stabilizer of Ag (Figure S7). Analysis of the UV−vis absorption spectra of ≪Ag-rGO≫ and ≪Ag-NrGO≫ NPs without PEG revealed the charge exchange rate to be ∼15.27 times higher in ≪Ag-NrGO≫ (∼1096.36) than in ≪Ag-rGO≫ (∼71.80) platform, demonstrating the pronounced catalytic effect of rGO due to the N-doped silver structure (Figure S8). In the presence of thiocyanate anions, Ag nanostructures undergo oxidation,[68,69] resulting in the formation of the sparingly soluble silver salt AgSCN(s)[70] and the release of an electron, $Ag + SCN^- \leftrightarrow AgSCN + e^-$. At high concentrations of thiocyanate, as in our case, AgSCN(s) can react with additional SCN^- anions and form higher-order soluble silver thiocyanate complexes $[Ag(SCN)y]^{1-y}$. Leaching of silver ions can be considered negligible because the isotropic or anisotropic dissolution of complexed silver nanostructures does not involve electrochemical oxidation processes.

3.4. Theoretical Modeling of H^+ Production by ≪Ibu-Ag-NrGO≫ in a Cervix Tumor. In this model, it is assumed that a cervix tumor is electrochemically treated with direct current in the use of electrodes with a surface modified by pristine ibuprofen, ≪Ibu-Ag≫, and ≪Ibu-Ag-NrGO≫ NPs, which are electrolyzed inside the tissue at an applied voltage of 0.53 to 0.60 V, resulting in H^+ production (Figure 3C,F,I). The process of H^+ production can be derived from oxygen evolution reaction close to the surface of the electrode at the contact with pristine ibuprofen and NPs with the highest concentration at 0.53 V. At this voltage, ≪Ibu-Ag-NrGO≫ NPs produced H^+ ions ∼13,2 times larger than pristine ibuprofen and ∼4,6 times larger than ≪Ibu-Ag≫. As the applied voltage increased up to 0.60 V, the produced amount of H^+ ions linearly decreased in all three types of these compounds with the highest rate on ≪Ibu-Ag-NrGO≫ of $\sim 1{,}5 \times 10^3$ (Figure 3C) in comparison with pristine ibuprofen ($\sim 1.2 \times 10^2$) (Figure 3F) and ≪Ibu-Ag≫ ($\sim 3.3 \times 10^2$) (Figure 3I). In contrast, the rate of decreased production of H^+ on bare Ag NPs was ∼36.0, and that on ≪Ag-NrGO≫ was $\sim 6.7 \times 10^2$ (Figure S9). Therefore, one can conclude that the catalytic efficiency of ibuprofen in ≪Ibu-Ag-NrGO≫ can be attributed to the complex effect caused by increased electron density of the ≪Ag-NrGO≫ platform. This is in agreement with the experimental results obtained in the study of the charge exchange reaction between hexacyanoferrate and thiosulfate ions (Figure 3B,E,H).

3.5. Theoretical Modeling of the Electromagnetic Field Strength Intensity and Power Flow Density Distribution by ≪Ibu-Ag-NrGO≫ Coupled to a Bioheat Equation in a Cervix Tumor under Microwave Irradiation. This type of modeling is related to the field of microwave chemotherapy at conditions of locally creating gradients of elevated electric field intensity in combination with the effect of complexed ibuprofen within ≪Ag-NrGO≫ under microwave irradiation (1.0×10^2−1.0×10^3 MHz, 10 W). The aim of the biophysical modeling is to find out the conditions of fastest electric field strength acceleration speed E ($V/m(Sm^{-1})$) and time-averaged power flow distribution P_{cervix} ($W/kg(Sm^{-1})$) on the surface of semiconductor NPs in comparison with pristine ibuprofen inside cervix tumor tissues. In this regard, Figure 4 shows the overall tendency of the nonlinear increase of the computed maximal magnitudes of the electric field strength intensity of pristine ibuprofen (Figure 4a), ≪Ibu-Ag≫ (Figure 4b), and ≪Ibu-Ag-NrGO≫ (Figure 4c) NPs according to their physical properties at increased values of the electrical conductivity in the studied range from 1 $\times 10^{-4}$ to 1×10^2 S/m under microwave irradiation.

The computed rate of the E_{max} magnitude changes versus the electrical conductivity in the range from 1×10^{-3} to 1×10^{-1} S/m in the selected microwave irradiation region was the highest on ≪Ibu-Ag-NrGO≫ NPs being $\sim 1.27 \times 10^8$ (Figure 4f) and with lower comparable rates on pristine ibuprofen ($\sim 6.68 \times 10^2$) and ≪Ibu-Ag≫ ($\sim 6.74 \times 10^2$) (Figure 4d,e). The computed rates of the total power dissipation density of bioheat flow distribution changes versus the electrical conductivity in the same selected range of σ were the highest on ≪Ibu-Ag≫ being $\sim 7.39 \times 10^3$ (Figure 4h) and with ≈1.1 times lower values on ≪Ibu-Ag-NrGO≫ ($\sim 6.83 \times 10^2$)

https://doi.org/10.1021/acsbiomaterials.2c01045
ACS Biomater. Sci. Eng. XXXX, XXX, XXX−XXX

(Figure 4i) and ≈2.0 times lower values on pristine ibuprofen (~3.63×10^2) (Figure 4g). The total power dissipation density P_{cervix} (W/kg) of bioheat flow exhibited the highest intensity at the tip of the electrode in all three compounds, and their surface dissipation zones at the slot were decreased in the following order: from ≪Ibu-Ag≫ (Figure 4k) to ≪Ibu-Ag-NrGO≫ (Figure 4l) and pristine ibuprofen (Figure 4j), indicating the pronounced effect of Ag. It is important to note that only on ≪Ibu-Ag-NrGO≫ NPs did the P_{cervix} dissipation of bioheat flow surface density profile showed the periodic appearance of local field changes in contrast to pristine ibuprofen and ≪Ibu-Ag≫.

4. CONCLUSIONS

A method of activation of pristine ibuprofen organic molecular crystals was demonstrated via ultrasonic (20 kHz) complexation of drug ligands with silver in nitrogen-doped oxidized graphene nanostructures (~50 nm). Ultrasound can cause the formation of an atomic Ag cluster structure in a complex with ibuprofen in ≪Ibu-Ag-NrGO≫ that is stabilized by intramolecular transconformational interaction with PEG, leading to an increase in the solubility of drug ligands inside NPs. In contrast to pristine ibuprofen, ≪Ibu-Ag≫ has a silver−aromatic complex and enhanced electronic transitions in the entire structure of NPs, which lead to a 4.5 times faster reaction rate in the oxidation of thiosulfate by hexacyanoferrate ions because of the acceleration of the charge transfer between the phenyl and carboxyl groups of ibuprofen molecules in a complex with Ag having C−O bonds. However, the same reaction can be catalyzed by ≪Ibu-Ag-NrGO≫ at a 42 times faster reaction rate than pristine ibuprofen by charge injection/ejection processes into and out of the surface of the individual semiconducting crystals. The electrokinetic activation of pristine ibuprofen can be caused by the overall increased electron density of ≪Ibu-Ag-NrGO≫ due to electronic $\pi c = c \rightarrow \pi c = c^*$ transitions in the altered phenyl ring and $\pi py \rightarrow \pi co^*$ in drug molecules between the phenyl ring and C−O bonds, groups in ≪NrGO≫ acting as electron donors, and an atomic Ag-cluster structure in a ferrocyanide−ibuprofen complex.

Theoretical modeling of H+ production by ≪Ibu-Ag-NrGO≫ in a cervix tumor tissue shows that the produced amount of H^+ ions decreased at a 12.5 times higher rate in ≪Ibu-Ag-NrGO≫ than in pristine ibuprofen at increased applied voltage from 0.53 to 0.60 V. Relevant to microwave chemotherapy of cervix tumor tissues, the computed maximal magnitudes of the electric field strength intensity of ≪Ibu-Ag-NrGO≫ undergo ~10^5 order higher changes than pristine ibuprofen or ≪Ibu-Ag≫ in the 100−1000 MHz range. The computed total power dissipation density of bioheat flow surface density profile showed the periodic appearance of local field changes only in ≪Ibu-Ag-NrGO≫ in contrast to pristine ibuprofen and ≪Ibu-Ag≫. This method can be successfully applied to activate various organic molecular crystals with pharmaceutical properties and determine the biophysical conditions of improved microwave chemotherapy of cervix tissues.

■ ASSOCIATED CONTENT

Supporting Information

The Supporting Information is available free of charge at https://pubs.acs.org/doi/10.1021/acsbiomaterials.2c01045.

Protocol of the synthesis of rGO; computed magnitudes of electrical conductivity and permittivity of cervix tissue in a microwave field in the frequency range from 1 to 1000 MHz; SEM images and energy dispersive X-ray fluorescence (EDX) spectrum of synthesized N-doped oxidized graphene; EDX spectrum of formed Ag-N-doped oxidized graphene with Ag 1.1 at. % (A) and 3.6 at. %; analysis of Raman spectra of pristine ibuprofen, ≪Ibu-Ag≫, ≪Ibu-Ag-NrGO≫, and ≪Ag-NrGO≫; UV−vis absorption spectra of aqueous solutions of 200 μL of 0.01 M $Fe(CN)_6^{3-}$ and 200 μL of 0.1 M $S_2O_3^{2-}$ during 45 min of reaction and the calibration plot of hexacyanoferrate concentration; UV−vis absorption spectra of the redox reaction between hexacyanoferrate and thiosulfate ions with PEG-coated ≪Ag-NrGO≫ and ≪NrGO≫, 5 mM $AgNO_3$ before and after stabilization by PEG, and ≪Ag-rGO≫ and ≪Ag-NrGO≫ without PEG; and computed concentration evolution of H^+ ions produced by Ag and ≪Ag-NrGO≫ inside the electrolyzed cervix tumor tissue in the applied voltage range from 0.53 to 0.60 V (PDF)

■ AUTHOR INFORMATION

Corresponding Author

Darya V. Radziuk − *Laboratory of Integrated Micro- and Nanosystems, Belarusian State University of Informatics and Radioelectronics, Minsk 220013, Republic of Belarus;* orcid.org/0000-0001-7287-4303; Email: radziuk@bsuir.by

Authors

Aleksey Drinevskyi − *Laboratory of Integrated Micro- and Nanosystems, Belarusian State University of Informatics and Radioelectronics, Minsk 220013, Republic of Belarus*

Evgenij Zelkovskyi − *Laboratory of Integrated Micro- and Nanosystems, Belarusian State University of Informatics and Radioelectronics, Minsk 220013, Republic of Belarus*

Viktar Abashkin − *Institute of Biophysics and Cell Engineering of National Academy of Sciences of Belarus, Minsk 220072, Republic of Belarus*

Dzmitry Shcharbin − *Institute of Biophysics and Cell Engineering of National Academy of Sciences of Belarus, Minsk 220072, Republic of Belarus*

Tamara Rysalskaya − *Laboratory of Integrated Micro- and Nanosystems, Belarusian State University of Informatics and Radioelectronics, Minsk 220013, Republic of Belarus*

Complete contact information is available at: https://pubs.acs.org/10.1021/acsbiomaterials.2c01045

Author Contributions

The manuscript was written through contributions of all authors.

Notes

The authors declare no competing financial interest.

■ ACKNOWLEDGMENTS

The authors acknowledge support by the Belarusian Republican Foundation for Fundamental Research grant SCIENTIST (BRFFR F22Y-007), B20SLKG-002, B21KORG-001, B21TUB-001, B21RM-045, and B21M-001 and Belarusian State Research grant nos. 21-3067 1.17, 21-3051 57 031.00, and 21-3163M.

REFERENCES

(1) Lagunas, L.; Bradbury, C. M.; Laszlo, A.; Hunt, C. R.; Gius, D. Indomethacin and ibuprofen induce Hsc70 nuclear localization and activation of the heat shock response in HeLa cells. *Biochem. Biophys. Res. Commun.* **2004**, *313*, 863−870.

(2) Shi, J.; Kantoff, P. W.; Wooster, R.; Farokhzad, O. C. Cancer nanomedicine: progress, challenges and opportunities. *Nat. Rev. Cancer.* **2017**, *17*, 20−37.

(3) Cui, W.; Li, J.; Decher, G. Self-assembled smart nanocarriers for targeted drug delivery. *Adv. Mater.* **2016**, *28*, 1302−1311.

(4) Yang, Y.; Achazi, K.; Jia, Y.; Wei, Q.; Haag, R.; Li, J. Complex assembly of polymer conjugated mesoporous silica nanoparticles for intracellular pH-responsive drug delivery. *Langmuir* **2016**, *32*, 12453−12460.

(5) Li, H.; Jia, Y.; Wang, A.; Cui, W.; Ma, H.; Feng, X.; Li, J. Self-assembly of hierarchical nanostructures from dopamine and polyoxometalate for oral drug delivery. *Chem. − Eur. J.* **2014**, *20*, 499−504.

(6) Yang, M.; Yang, T.; Mao, C. Enhancement of photodynamic cancer therapy by physical and chemical factors. *Angew. Chem. Int. Ed. Engl.* **2019**, *58*, 14066−14080.

(7) Chen, J.; Zhu, Y.; Wu, C.; Shi, J. Nanoplatform-based cascade engineering for cancer therapy. *Chem. Soc. Rev.* **2020**, *49*, 9057−9094.

(8) Wang, J.; Wang, D.; Yan, H.; Tao, L.; Wei, Y.; Li, Y.; Wang, X.; Zhao, W.; Zhang, Y.; Zhao, L.; Sun, X. An injectable ionic hydrogel inducing high temperature hyperthermia for microwave tumor ablation. *J. Mater. Chem. B* **2017**, *5*, 4110−4120.

(9) Tan, L.; Tang, W.; Liu, T.; Ren, X.; Fu, C.; Liu, B.; Ren, J.; Meng, X. Biocompatible hollow polydopamine nanoparticles loaded ionic liquid enhanced tumor microwave thermal ablation in vivo. *ACS Appl. Mater. Interfaces* **2016**, *8*, 11237−11245.

(10) Pesic, M.; Greten, F. R. Inflammation and cancer: tissue regeneration gone awry. *Curr. Opin. Cell Biol.* **2016**, *43*, 55−61.

(11) Dong, Q.; Wang, X.; Hu, X.; Xiao, L.; Zhang, L.; Song, L.; Xu, M.; Zou, Y.; Chen, L.; Chen, Z.; Tan, W. Simultaneous application of photothermal therapy and an anti-inflammatory prodrug using pyrene-aspirin-loaded gold nanorod graphitic nanocapsules. *Angew. Chem. Int. Ed. Engl.* **2018**, *57*, 177−181.

(12) Wu, Q.; Yu, J.; Li, M.; Tan, L.; Ren, X.; Fu, C.; Chen, Z.; Cao, F.; Ren, J.; Li, L.; Liang, P.; Zhang, Y.; Meng, X. Nanoengineering of nanorattles for tumor treatment by CT imaging-guided simultaneous enhanced microwave thermal therapy and managing inflammation. *Biomaterials* **2018**, *179*, 122−133.

(13) Eden, B. D.; Rice, A. J.; Lovett, T. D.; Toner, O. M.; Geissler, E. P.; Bowman, W. E.; Young, S. C. Microwave-assisted synthesis and in vitro stability of N-benzylamide non-steroidal anti-inflammatory drug conjugates for CNS delivery. *Bioorg. Med. Chem. Lett.* **2019**, *29*, 1487−1491.

(14) Tiwari, A. D.; Panda, S. S.; Girgis, A. S.; Sahu, S.; George, R. F.; Srour, A. M.; La Starza, B.; Asiri, A. M.; Hall, C. D.; Katritzky, A. R. Microwave assisted synthesis and QSAR study of novel NSAID acetaminophen conjugates with amino acid linkers. *Org. Biomol. Chem.* **2014**, *12*, 7238−7249.

(15) Shi, N.-Q.; Lai, H.-W.; Zhang, Y.; Feng, B.; Xiao, X.; Zhang, H.-M.; Li, Z.-Q.; Qi, X.-R. On the inherent properties of Soluplus® and its application in ibuprofen solid dispersions generated by microwave-quench cooling technology. *Pharm. Dev. Technol.* **2018**, *23*, 573−586.

(16) Moneghini, M.; Bellich, B.; Baxa, P.; Princivalle, F. Microwave generated solid dispersions containing ibuprofen. *Int. J. Pharm.* **2008**, *361*, 125−130.

(17) Hempel, N.-J.; Knopp, M. M.; Berthelsen, R.; Zeitler, J. A.; Löbmann, K. The influence of drug and polymer particle size on the in situ amorphization using microwave irradiation. *Eur. J. Pharm. Biopharm.* **2020**, *149*, 77−84.

(18) Alshehri, S.; Shakeel, F.; Ibrahim, M.; Elzayat, E.; Altamimi, M.; Shazly, G.; Mohsin, K.; Alkholief, M.; Alsulays, B.; Alshetaili, A.; Alshahrani, A.; Almalki, B.; Alanazi, F. Influence of the microwave technology on solid dispersions of mefenamic acid and flufenamic acid. *PLoS One* **2017**, *12*, 1−18.

(19) Kim, J. M.; Ko, D.; Oh, J.; Lee, J.; Hwang, T.; Jeon, Y.; Antink, W. H.; Pia, Y. Electrochemically exfoliated graphene as a novel microwave susceptor: the ultrafast microwave-assisted synthesis of carbon coated silicon-graphene film as lithium-ion battery anode. *Nanoscale* **2017**, *9*, 15582−15590.

(20) Ahmad, R.; Mahmoudi, T.; Ahn, M.-S.; Yoo, J.-Y.; Hahn, Y.-B. Fabrication of sensitive non-enzymatic nitrite sensor using silver-reduced graphene oxide nanocomposite. *J. Colloid Interface Sci.* **2018**, *516*, 67−75.

(21) Zhao, R.; Lv, M.; Li, Y.; Sun, M.; Kong, W.; Wang, L.; Song, S.; Fan, C.; Jia, L.; Qiu, S.; Sun, Y.; Song, H.; Hao, R. Stable nanocomposite based on PEGylated and silver nanoparticles loaded graphene oxide for long-term antibacterial activity. *ACS Appl. Mater. Interfaces* **2017**, *9*, 15328−15341.

(22) de Almeida, G. C.; Mohallem, N. D. S.; Viana, M. M. Ag/GO/TiO_2 nanocomposites: the role of the interfacial charge transfer for application in photocatalysis. *Nanotechnology* **2022**, *33*, No. 035710.

(23) Perry, R. H. Theoretical study of the adsorption of analgesic environmental pollutants on pristine and nitrogen-doped graphene nanosheets. *Phys. Chem. Chem. Phys.* **2021**, *23*, 1221−1233.

(24) Youn, H.-C.; Bak, S.-M.; Kim, M.-S.; Jaye, C.; Fischer, D. A.; Lee, C.-W.; Yang, X.-Q.; Roh, K. C.; Kim, K.-B. High-surface-area nitrogen-doped reduced graphene oxide for electric double-layer capacitors. *ChemSusChem* **2015**, *8*, 1875−1884.

(25) Wang, Y.; Shao, Y.; Matson, D. W.; Li, J.; Lin, Y. Nitrogen-doped graphene and its application in electrochemical biosensing. *ACS Nano* **2010**, *4*, 1790−1798.

(26) Cui, L.; Huan, Y.; Shan, J.; Liu, B.; Liu, J.; Xie, H.; Zhou, F.; Gao, P.; Zhang, Y.; Liu, Z. Highly conductive nitrogen-doped vertically oriented graphene toward versatile electrode-related applications. *ACS Nano* **2020**, *14*, 15327−15335.

(27) Xu, H.; Ma, L.; Jin, Z. Nitrogen-doped graphene: Synthesis, characterizations and energy applications. *J. Energy Chem.* **2018**, *27*, 146−160.

(28) Yan, P.; Shu, S.; Zou, L.; Liu, Y.; Li, J.; Wei, F. Density functional theory study of active sites on nitrogen-doped graphene for oxygen reduction reaction. *R. Soc. Open Sci.* **2021**, *8*, 210272.

(29) Nørskov, J. K.; Rossmeisl, J.; Logadottir, A.; Lindqvist, L.; Kitchin, J. R.; Bligaard, T.; Jónsson, H. Origin of the overpotential for oxygen reduction at a fuel-cell cathode. *J. Phys. Chem. B* **2004**, *108*, 17886−17892.

(30) Zhou, R.; Qiao, S. Z. Silver/nitrogen-doped graphene interaction and its effect on electrocatalytic oxygen reduction. *Chem. Mater.* **2014**, *26*, 5868−5873.

(31) Yue, M.; Si, J.; Yan, L.; Yu, Y.; Hou, X. Enhanced nonlinear optical properties of reduced graphene oxide decorated with silver nanoparticles. *Opt. Mater. Express* **2018**, *8*, 698−703.

(32) Chen, Y.; Tao, J.; Hammami, M. A.; Hoang, P.; Khashab, N. M. Self-assembly of single-crystal silver microflakes on reduced graphene oxide and their use in ultrasensitive sensors. *Adv. Mater. Interfaces* **2016**, *3*, 1500658.

(33) Mohammadi, Z.; Entezari, M. H. Sono-synthesis approach in uniform loading of ultrafine Ag nanoparticles on reduced graphene oxide nanosheets: An efficient catalyst for the reduction of 4-Nitrophenol. *Ultrason. Sonochem.* **2018**, *44*, 1−13.

(34) Neppolian, B.; Wang, C.; Ashokkumar, M. Sonochemically synthesized mono and bimetallic Au-Ag reduced graphene oxide based nanocomposites with enhanced catalytic activity. *Ultrason. Sonochem.* **2014**, *21*, 1948−1953.

(35) Xiong, S.; Zhou, J.; Wu, J.; Li, H.; Zhao, W.; He, C.; Liu, Y.; Chen, Y.; Fu, Y.; Duan, H. High performance acoustic wave nitrogen dioxide sensor with ultraviolet activated 3D porous architecture of Ag-decorated reduced graphene oxide and polypyrrole aerogel. *ACS Appl. Mater. Interfaces* **2021**, *13*, 42094−42103.

(36) Xu, H.; Zeiger, B. W.; Suslick, K. S. Sonochemical synthesis of nanomaterials. *Chem. Soc. Rev.* **2013**, *42*, 2555−2567.

(37) Kim, H. N.; Suslick, K. S. Sonofragmentation of organic molecular crystals vs strength of materials. *J. Org. Chem.* **2021**, *86*, 13997−14003.

https://doi.org/10.1021/acsbiomaterials.2c01045
ACS Biomater. Sci. Eng. XXXX, XXX, XXX−XXX

(38) Manish, M.; Harshal, J.; Anant, P. Melt sonocrystallization of ibuprofen: effect on crystal properties. *Eur. J. Pharm. Sci.* **2005**, *25*, 41−48.
(39) Eder, R. J. P.; Schrank, S.; Besenhard, M. O.; Roblegg, E.; Gruber-Woelfler, H.; Khinast, J. G. Continuous sonocrystallization of acetylsalicylic acid (ASA): control of crystal size. *Cryst. Growth Des.* **2012**, *12*, 4733−4738.
(40) Bučar, D.-K.; Elliott, J. A.; Eddleston, M. D.; Cockcroft, J. K.; Jones, W. Sonocrystallization yields monoclinic paracetamol with significantly improved compaction behavior. *Angew. Chem., Int. Ed.* **2015**, *54*, 249−253.
(41) Zhu, J.-J.; Qiu, Q.-F.; Wang, H.; Zhang, J.-R.; Zhu, J.-M.; Chen, Z.-Q. Synthesis of silver nanowires by a sonoelectrochemical method. *Inorg. Chem. Commun.* **2002**, *5*, 242−244.
(42) Chen, W.; Zhang, J.; Cai, W. Sonochemical preparation of Au, Ag, Pd/SiO_2 mesoporous nanocomposites. *Scr. Mater.* **2003**, *48*, 1061−1066.
(43) Kumar, R. V.; Palchik, O.; Koltypin, Y.; Diamant, Y.; Gedanken, A. Sonochemical synthesis and characterization of Ag_2S/PVA and CuS/PVA nanocomposite. *Ultrason. Sonochem.* **2002**, *9*, 65−70.
(44) Jiang, L.-P.; Xu, S.; Zhu, J.-M.; Zhang, J.-R.; Zhu, J.-J.; Chen, H.-Y. Ultrasonic-assisted synthesis of monodisperse single-crystalline silver nanoplates and gold nanorings. *Inorg. Chem.* **2004**, *43*, 5877−5883.
(45) Xu, H.; Suslick, K. S. Sonochemical synthesis of highly fluorescent Ag nanoclusters. *ACS Nano* **2010**, *4*, 3209−3214.
(46) Gottesman, R.; Shukla, S.; Perkas, N.; Solovyov, L. A.; Nitzan, Y.; Gedanken, A. Sonochemical coating of paper by microbiocidal silver nanoparticles. *Langmuir* **2011**, *27*, 720−726.
(47) Chen, D.; Yoo, S. H.; Huang, Q.; Ali, G.; Cho, S. O. Sonochemical synthesis of Ag/AgCl nanocubes and their efficient visible-light-driven photocatalytic performance. *Chem. − Eur. J.* **2012**, *18*, 5192−5200.
(48) Shi, J.; Wang, L.; Zhang, J.; Ma, R.; Gao, J.; Liu, Y.; Zhang, C.; Zhang, Z. A tumor-targeting near-infrared laser-triggered drug delivery system based on GO@Ag nanoparticles for chemo-photothermal therapy and X-ray imaging. *Biomaterials* **2014**, *35*, 5847−5861.
(49) Das, M. R.; Sarma, R. K.; Saikia, R.; Kale, V. S.; Shelke, M. V.; Sengupta, P. Synthesis of silver nanoparticles in an aqueous suspension of graphene oxide sheets and its antimicrobial activity. *Colloids Surf., B* **2011**, *83*, 16−22.
(50) Abdelrazik, A. S.; Tan, K. H.; Aslfattahi, N.; Saidur, R.; Al-Sulaiman, F. A. Optical properties and stability of water-based nanofluids mixed with reduced graphene oxide decorated with silver and energy performance investigation in hybrid photovoltaic/thermal solar systems. *Int. J Energy Res.* **2020**, *44*, 11487−11508.
(51) Pasricha, R.; Gupta, S.; Srivastava, A. K. A facile and novel synthesis of Ag−graphene-based nanocomposites. *Small* **2009**, *5*, 2253−2259.
(52) Marcano, D. C.; Kosynkin, D. V.; Berlin, J. M.; Sinitskii, A.; Sun, Z.; Slesarev, A.; Alemany, L. B.; Lu, W.; Tour, J. M. Improved synthesis of graphene oxide. *ACS Nano* **2010**, *4*, 4806−4814.
(53) Nordenström, B. E. W. *Biologically closed electrical circuits: clinical, experimental and theoretical evidence for an additional circulatory system*; Nordic Medical Publications, Stockholm, 1983.
(54) Saito, K.; Taniguchi, T.; Yoshimura, H.; Ito, K. Estimation of SAR distribution of a tip-split array applicator for microwave coagulation therapy using the finite element method. *IEICE Trans. Electronics* **2001**, *E84.C*, 948−954.
(55) Ferrari, A. C.; Robertson, J. Interpretation of Raman spectra of disordered and amorphous carbon. *Phys. Rev. B* **2000**, *61*, 14095−14107.
(56) Ferreira, E. H. M.; Moutinho, M. V.; Stavale, F.; Lucchese, M. M.; Capaz, R. B.; Achete, C. A.; Jorio, A. Evolution of the Raman spectra from single-, few-, and many-layer graphene with increasing disorder. *Phys. Rev. B* **2010**, *82*, No. 125429.
(57) Perumbilavil, S.; Sankar, P.; Priya Rose, T.; Philip, R. White light Z-scan measurements of ultrafast optical nonlinearity in reduced graphene oxide nanosheets in the 400−700nm region. *Appl. Phys. Lett.* **2015**, *107*, No. 051104.
(58) Tuinstra, F.; Koenig, J. L. Raman spectrum of graphite. *J. Chem. Phys.* **1970**, *53*, 1126−1130.
(59) Hall, R. T.; Pimentel, G. C. Isomerization of nitrous acid: An infrared photochemical reaction. *J Chem. Phys.* **1963**, *38*, 1889−1897.
(60) Fleischmann, M.; Hendra, P. J.; McQuillan, A. J. Raman spectra of pyridine adsorbed at a silver electrode. *Chem. Phys. Lett.* **1974**, *26*, 163−166.
(61) Knight, D. S.; White, W. B. Characterization of diamond films by Raman spectroscopy. *J. Mater. Res.* **1989**, *4*, 385−393.
(62) Sehested, K.; Corfitzen, H.; Christensen, H. C.; Hart, E. J. Rates of reaction of oxygen(1-) ions, hydroxyl radicals, and atomic hydrogen with methylated benzenes in aqueous solution. Optical spectra of radicals. *J. Phys. Chem.* **1975**, *79*, 310−315.
(63) Soares, F. L. F.; Carneiro, R. L. Evaluation of analytical tools and multivariate methods for quantification of co-former crystals in ibuprofen-nicotinamide co-crystals. *J. Pharm. Biomed. Anal.* **2014**, *89*, 166−175.
(64) Bonora, S.; Pisi, A.; Ottani, S.; Cesini, D.; Maris, A.; Di Foggia, M. Raman and SERS study on ibuprofen metal complexes with biomedical interest. *Vib. Spectrosc.* **2014**, *73*, 45−55.
(65) Núñez, C.; Fernández-Lodeiro, A.; Fernández-Lodeiro, J.; Carballo, J.; Capelo, J. L.; Lodeiro, C. Synthesis, spectroscopic studies and in vitro antibacterial activity of ibuprofen and its derived metal complexes. *Inorg. Chem. Commun.* **2014**, *45*, 61−65.
(66) Shakhtshneider, T. P.; Vasiltchenko, M. A.; Politov, A. A.; Boldyrev, V. V. The mechanochemical preparation of solid disperse systems of ibuprofen-polyethylene glycol. *Int. J. Pharm.* **1996**, *130*, 25−32.
(67) Alexander, J. J.; Gray, H. B. Electronic structures of hexacyanometalate complexes. *J. Am. Chem. Soc.* **1968**, *90*, 4260−4271.
(68) Majed, Y. A. The kinetics of some reactions involving ferricyanide. Thesis, the University of London, 1963.
(69) Wonnera, K.; Eversa, M. V.; Tschulik, K. The electrochemical dissolution of single silver nanoparticles enlightened by hyperspectral dark-field microscopy. *Electrochim. Acta* **2019**, *301*, 458−464.
(70) Comey, A. M.; Hahn, D. A. *A Dictionary of chemical solubilities: inorganic*; Macmillan Company, 1921.

https://doi.org/10.1021/acsbiomaterials.2c01045
ACS Biomater. Sci. Eng. XXXX, XXX, XXX−XXX